AD-A092 533 BRISTOL UNIV (ENGLAND) DEPT OF AERONAUTICAL ENGINEERING F/G 20/4
PRESSURES ON A SLENDER, AXISYMMETRIC BODY AT HIGH ANGLE OF ATTA--ETC(U)
OCT 80 P C DEXTER, J W FLOWER DA-ERO-77-G-073
UNCLASSIFIED PCD/8001 NL

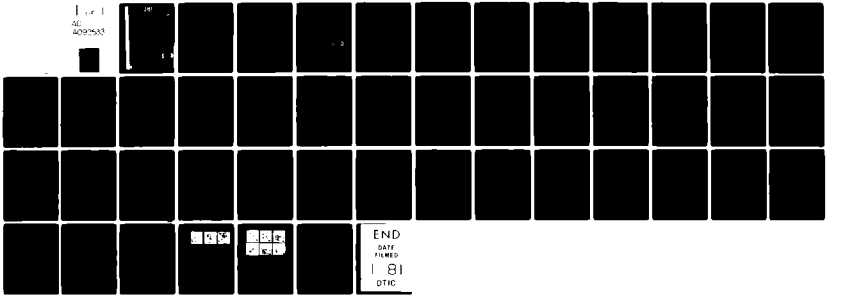

Report No. FED 8001

UNIVERSITY OF BRISTOL

DEPARTMENT OF
AERONAUTICAL ENGINEERING

PRESSURES ON A SLENDER, AXISYMMETRIC BODY AT HIGH ANGLE OF ATTACK IN A VERY LOW TURBULENCE LEVEL AIR STREAM

Third Annual Report
by
P. C. Dexter and J. W. Flower

October 1980

U.S. ARMY EUROPEAN RESEARCH OFFICE
AND
U.S. AIR FORCE EUROPEAN OFFICE OF
AEROSPACE RESEARCH AND DEVELOPMENT

London, England

Grant Number DA-ERO-77-G-073

UNCLASSIFIED

SECURITY CLASSIFICATION OF THIS PAGE (When Data Entered) (14) PCD/80Ø1

REPORT DOCUMENTATION PAGE

READ INSTRUCTIONS BEFORE COMPLETING FORM

1. REPORT NUMBER

2. GOVT ACCESSION NO. AD-A092533

3. RECIPIENT'S CATALOG NUMBER (9)

4. TITLE (and Subtitle) (6)
Pressures on a Slender, Axisymmetric Body at High Angle of Attack in a Very Low Turbulence Level Air Stream

5. TYPE OF REPORT & PERIOD COVERED
Third Annual Report no. 3
May 79 — June 80,

6. PERFORMING ORG. REPORT NUMBER

7. AUTHOR(s) (10)
P.C. Dexter
J.W. Flower

8. CONTRACT OR GRANT NUMBER(s) (15)
DAERO-77-G-Ø73

9. PERFORMING ORGANIZATION NAME AND ADDRESS
University of Bristol, Dept. of Aero. Eng., Queen's Building, University Walk, Bristol, BS8 1TR, England.

10. PROGRAM ELEMENT, PROJECT, TASK AREA & WORK UNIT NUMBERS (16)
IT161102BH57-06 (17) Ø6

11. CONTROLLING OFFICE NAME AND ADDRESS (11)
U.S. Army Research & Standardisation Group (Eur)
Box 65,
FPO NY 09510

12. REPORT DATE
October 1980

13. NUMBER OF PAGES
43

14. MONITORING AGENCY NAME & ADDRESS (if different from Controlling Office) (12) 46

15. SECURITY CLASS. (of this report)
Unclassified

15a. DECLASSIFICATION/DOWNGRADING SCHEDULE

16. DISTRIBUTION STATEMENT (of this Report)

Approved for Public Release; Distribution Unlimited.

17. DISTRIBUTION STATEMENT (of the abstract entered in Block 20, if different from Report)

Approved for Public Release; Distribution Unlimited

18. SUPPLEMENTARY NOTES

19. KEY WORDS (Continue on reverse side if necessary and identify by block number)

High Angle of Attack	Low Turbulence
Vortex Shedding	Bodies of Revolution
Side Forces at Large Angle of Attack	Low Speed
Roll Angle Dependency	Flow Visualisation

20. ABSTRACT (Continue on reverse side if necessary and identify by block number)

This report describes the work and results of the third year on this contract to investigate the pressures on slender bodies at high incidence. Results are presented of experimentally measured pressures on a model consisting of an axisymmetric cylindrical body with two interchangeable ogive nose sections in a low speed, low turbulence level freestream. Incidences up to 90° and the full roll angle range were covered. The results show a dependence on roll angle but indicate that a 'universal regular' state may

DD FORM 1 JAN 73 1473 EDITION OF 1 NOV 65 IS OBSOLETE

UNCLASSIFIED 409571

SECURITY CLASSIFICATION OF THIS PAGE (When Data Entered)

Abstract (continued)

exist for the flow, with intermediate states also being possible. The 'regular' state involves the maximum local force values. Local side force and normal force distributions are presented for a number of cases. A suitable test technique to attain scatter-free reproducible data is proposed. Details of flow visualisation using a wool tuft grid are given.

SUMMARY

This report describes the work and results of the third year on this contract to investigate the pressures on slender bodies at high incidence. Results are presented of experimentally measured pressures on a model consisting of an axisymmetric cylindrical body with two interchangeable ogive nose sections in a low speed, low turbulence level freestream. Incidences up to 90° and the full roll angle range were covered. The results show a dependence on roll angle but indicate that a 'universal regular' state may exist for the flow, with intermediate states also being possible. The 'regular' state involves the maximum local force values. Local side force and normal force distributions are presented for a number of cases. A suitable test technique to attain scatter-free reproducible data is proposed. Details of flow visualisation using a wool tuft grid are given.

TABLE OF CONTENTS

1. INTRODUCTION

It has been known for over twenty-five years that axisymmetric bodies are subject to side forces when inclined at high angles of incidence to a uniform stream. Since the late 1960's much experimental work has been reported on high incidence research as the need to enlarge the flight envelopes of missiles and bodies arose. A large number of references are mentioned by Ericsson and Reding (ref. 1). However, much of the work showed inconsistencies, and although certain trends emerged it was not difficult to find exceptions. Often large discrepancies were found between results of different workers. The extent of the problem was illustrated by the study of Wardlaw and Morrison (ref. 2) in which they were forced to try correlating side force measurements by linear regression. They found that ordinary conventional flow and geometry parameters were insufficient owing to the wide margin of differences in available data.

The present study was originated in order to try to understand why there should be such large differences in data, and hence to find ways in which reliable data could be produced.

Previous experimental studies had given some clues as to the origins of the difficulties. It had been found by most experimenters who looked for it that the side force might vary in both size and direction at different roll angles. It was also found by Lamont and Hunt (refs. 3 and 4) that unsteadiness, both from the mounting system and the freestream turbulence, caused experimental difficulties. Their transient records showed differences in switching pattern with roll angle while the inferred unswitched levels seemed to be unaffected. They postulated that the observed influence of roll angle on the time-averaged results would be eliminated if the unsteadiness were eliminated.

The initial work of this study set out to check on Lamont and Hunt's (refs. 3 and 4) notion of the importance of freestream turbulence, using a rigidly mounted model in a very low turbulence level freestream. The model used was the same as that used by Lamont and Hunt and at the same subcritical Reynolds numbers. It was found, as reported in ref. 5, that freestream turbulence did have a significant effect on the time-dependent pressures on the body, but that there was still a roll angle variation. The mean value of the measured pressures was changing as the roll angle changed, but there were no large variations in the time-dependent pressures as Lamont and Hunt had observed in their tests. Hence the change in mean level was not due to the variation in switching pattern as they had suggested, but was perhaps vice-versa.

Knowing that there was still a roll angle variation even in a very low turbulence freestream, an effort was made to see if this could be eliminated using an accurately manufactured model. It was shown (ref. 6) that although it may not be impossible, it was certainly very difficult,

and for most applications it is likely that there will be a roll angle dependence.

Hence this report gives more information, in addition to that of ref. 6, on the work which has been conducted into determining the effects of the roll angle dependence, and of how reliable data may be obtained at high angles of incidence.

The work has been conducted by measuring pressure distributions over the model body. This method, although slower than force measurements, produces much more information concerning the flow around the model. It is possible, for instance, by comparing the pressure distribution at a given model station to that around a circular cylinder at 90° to a uniform flow, to determine that all these tests were performed with laminar separation. As mentioned in the text, force measurements may overlook some important feature of the flow which may even lead to incorrect conclusions being drawn.

Because a new contract for another year's study has been granted, some of the most recent tests which have not yet been processed and analysed are not included in this report. The results will be included in reports under the new contract.

2. APPARATUS

The work reported here was conducted in the 4 ft x 3 ft Experimental Low Turbulence Wind Tunnel at R.A.E. Farnborough. This tunnel has a contraction ratio of 31·1 : 1 with a working section of 1·2 m x 0·9 m, which has a freestream turbulence level of about 0·01% over the majority of its cross-sectional area. The maximum tunnel speed is about 250 ft/sec (about 75 m/sec).

The model used consists basically of several 51 mm diameter screw-in sections which form a nose-cylindrical body configuration. The nose shape used for all the tests so far has been a fineness-ratio 3 tangent ogive. The measurement part of the model is constructed in five identical sections, each 1 diameter long and housing two measurement stations. At each measurement station there are 36 pressure tappings at 10^{o} intervals around the body and each tapping has narrow bore pressure tubing connected to it.

The nose section can screw directly into the measurement section or can be attached via a dummy section (as in fig. 1) which effectively increases the length of the measurement section. The dummy section is carefully made to ensure that the roll angle of the nose relative to the measurement section is unchanged, whether the dummy is used or not.

The measurement section is screwed into the support section which is held by the model support clamps. A new system of model support has been used in these latest tests over the past year. Instead of the support clamps directly gripping the support body they have been used to grip on roller bearings which are a tight fit on the support body. This has enabled the model to be rolled whilst still being firmly held and with the tunnel running (see fig. 2). The model support clamps are rigidly held by 51 mm diameter steel pylons to the roof and floor of the wind tunnel which is braced externally against a steel framework. The model rotates in a horizontal plane to achieve incidence. Roll angle is controlled by means of a worm driven by a flexible cable. The worm engages on a gear mounted on the rear of the body. Roll angle is read directly from a scale on the model support body.

The 360 tubes from the pressure tappings are led through the inside of the model, along the tunnel floor and into the observation room. They terminate in a total of 10 Scanivalve rings which can be connected in turn to a single Scanivalve controlled by a data-logger. The rings are blanked off when not connected to the Scanivalve. The pressure from each tube is read 3 times by the data-logger and then stored on paper tape for later analysis on a computer at Bristol University. The readings so obtained allow the pressure distribution over most of the body to be found and by integration the local side and normal forces can be determined.

Other tests have been performed with a wool tuft grid mounted behind the body. The basic dimensions of the grid and its positioning are shown in

fig. 3. The grid can be moved independently of the body, which can also be rolled whilst the grid is in position. The flow patterns produced have been recorded photographically and used in analysing the pressure and force results.

3. TESTS CONDUCTED

The tests during this period have all been conducted at a Reynolds number of 10^5 where Reynolds number is defined as $U\,d\,\mathrm{cosec}\,\alpha/\nu$ and U is freestream velocity, d is the diameter of the cylindrical section of the model, ν is the kinematic viscosity and α is the angle of incidence. This definition has been used throughout the investigation and a justification for its use is given by Lamont and Hunt (refs. 3 and 4). The most appropriate definition is by no means settled and alternative views may be found (refs. 7, 8 and 9). However, it was always intended that this investigation be performed at subcritical Reynolds numbers so that the results would not be affected by turbulent re-attachment and the pressure distributions obtained support this.

The other major parameters to be altered were angle of incidence α, roll angle ϕ and axial location of measuring station x/d. Additionally, another nose section was made to the same nominal dimensions as the first, a fineness ratio three tangent ogive. Obviously, although the basic shape is the same, the detail geometry such as machining imperfections will be different between the old and new noses. Results are presented from tests with both of these.

4. PRESENTATION AND DISCUSSION OF RESULTS

The pressures were measured by means of a Setra pressure transducer. The signal was monitored continually by means of a digital voltmeter and also passed through a low pass filter. The output from this filter was monitored using an oscilloscope and was also used as the input to a data logger which recorded the readings on paper tape. The data logger and Scanivalve were under microprocessor control.

The paper tape recordings were used to transfer the data onto the Bristol University mainframe computer which was programmed to produce tables of pressure coefficients and to integrate these pressures to give local side force and normal force values. The pressure readings from the 360 tubes were generally acceptable apart from 3 tubes (not close together) which always gave erroneous results. These were probably leaking somewhere inside the body of the model, but it was not possible to strip the model without risk of damage to other tubes. Instead, the readings for the tubes were 'corrected' (by interpolation) before the force calculations were performed.

4.1 50° Incidence

Much of the testing has been performed at 50° incidence because this generates strong, steady flowfields which are well into the asymmetric flow regime.

Tests were performed at roll angle intervals of 30° covering the full roll range, making 12 different angles altogether. A typical result is shown in fig. 4 which plots the variation of both local normal force and local side force against distance from model nose tip. It is worth noting the good agreement at $x/d = 7{\cdot}5$ and $8{\cdot}0$ between repeated points. These are obtained because the model without the dummy section in use gives results from $x/d = 3{\cdot}5$ to $x/d = 8{\cdot}0$ and with the dummy section the results span $x/d = 7{\cdot}5$ to $x/d = 12{\cdot}0$. The good agreement shows that the introduction of the dummy does not affect the flow over the model significantly. All the results are completely repeatable.

The local side force is seen to have a cyclic nature, as would be expected from the flow pattern which exhibits cyclic shedding of vortices with variation along the body length.

The initial flow asymmetry and hence start of the side force distribution is occurring over the nose section of the model and hence no measurements are available, but it can be seen that there are at least three half-cycles to the distribution. Discussion later will centre on the first half-cycle (or second half-cycle). The numbering starts from nearest the nose.

Such distributions have been obtained for at least all 12 roll angles for both noses: however, for clarity and to make the important conclusions it is not necessary to include all these results.

Fig. 5 shows typical side force distributions for a number of cases covering the body length x/d = 3·5 to x/d = 8·0. Note that there are two cases which are virtually identical and one which is the mirror image of these, which would arise from a mirror image flow pattern around and behind the body. These states are found to be the most commonly occurring throughout the roll angle range and are also associated with the largest side forces. Two other curves are also shown which represent states intermediate between the two hands of the most common state.

To represent the variation of the side force pattern throughout the roll angle range, the maximum value occurring in the first half-cycle of the distributions has been plotted against roll angle in fig. 6 for both noses. The major point to note in this figure is that both distributions have significant ranges over which the value of $C_{y_{max}}$ is around 2·0 (or in the mirror image state). This corresponds to the most commonly occurring state, or the 'regular' state. Other states are possible, but these are always intermediate with lower associated forces. The fact that the 'regular' state is the same for both noses tends to suggest that it is a 'universal' state in that it would be repeatable on any model of similar design. Provided a roll angle scan were performed, any fineness ratio three ogive nose in conjunction with a cylindrical body should produce the same 'universal regular' state. It is also possible to get just about any intermediate state too, even one with virtually no side force as shown in fig. 7.

It is interesting to compare the pressure distributions at certain stations on the body for the two extremes of a 'regular' high side force case (fig. 8) to that of the low side force case, fig. 9. It can be seen that with the low side force (fig. 9) the pressure distribution around the body remains symmetrical. The flow separates from the body at angular positions which are consistent with laminar flow and rolls up in two symmetric vortices which impinge on the body at the rearmost point causing a sudden pressure recovery. This is shown at both axial stations considered. However, the situation is somewhat different for the 'regular' case of fig. 8. Again, the separation points are consistent with laminar flow, but the distributions are highly asymmetric. At the two axial positions shown the side forces are in opposite directions. Each distribution is associated with one dominant vortex behind the body causing low pressure on one side of the body, due to high velocities, and higher pressure on the other.

Although the side force distributions vary with roll angle, it has been possible to correlate these variations to a certain extent. The greater the value of the maximum side force in the first half-cycle, the nearer to the model nose tip it occurs, and the nearer the nose is the first node point of the distribution. These trends are shown in fig. 10 and 11 which correlate the value of the first side force peak against its axial position in fig. 10 and against the first node in fig. 11. Results are taken from both noses. It is probable that any result obtained from similar tests with a similar model would agree with this correlation. Such correlations could also be done for other parts of the distribution and at other incidences,

hence there is a basis for the formulation of a prediction method. It is most likely though that any project engineer would be mainly interested in the case with the maximum side forces, the 'regular' case.

4.2 Other Incidences

Investigations of a similar nature have taken place at other incidences (α = 35°, 40°, 60° and 65°) and roll angles for just the old nose. The full roll angle range has been covered at α = 35° and α = 65°, and selected roll angles at α = 40° and α = 60°.

Typical results are shown in figs. 12 to 15 which show local side and normal force values at ϕ = 0° for each other incidence. It will be noticed that for 35° incidence the measurements cover only the first half-cycle of the side force distribution, but as incidence increases so more of the distribution is included. This is because the vortex flowfield developed over the body is dependent on incidence. The greater the incidence angle, the more closely packed the vortices become. They tend to migrate forward on the body towards and onto the nose. Hence the measurements at higher incidence angles omit some or all of the first half-cycle of the distribution and show a greater number of the remaining half-cycles. It can be seen that each successive half-cycle tends to have a smaller magnitude than its predecessor, incidating the decaying strengths of the successive vortices as they are shed from the body.

It has been found that the roll angle variation obtained at 50° incidence is generally repeated at the other incidences too. Fig. 16 shows the variation of the first half-cycle peak value with roll angle for incidences of 35°, 40° and 50°. Fig. 17 shows the same, but for the second half-cycle at incidences of 40°, 50°, 60° and 65° (note that the second half-cycle is always of opposite sign to the first half-cycle). It can be seen that the roll angle variation remains very similar throughout the incidence range, the 'handedness' of the distribution and the regions near the 'regular' state being in good agreement. It would also appear that as the incidence increases, the more near to a 'square wave type' the distribution becomes. At lower incidences the variation with roll angle can be quite gentle, whereas at higher incidences it tends to be more sharp, polarising to either one or other of the hands of the 'regular' state. This suggests that once the 'regular' state has been found by performing a roll angle scan at a moderate incidence, the same roll position can be used to obtain the 'regular' state results throughout the incidence range.

4.3 Normal Force

Although most of this investigation has been concerned with side forces at high incidence the variation of local normal force has been obtained at the same time. Generally, the local normal force is not

greatly influenced by the vortex flowfield developed by the body.

Where the side force showed a cyclic behaviour with successive half-cycles of diminishing magnitude, the effect on the normal force is not so large but is significant. Fig. 4 shows how both vary along the body length for a 'regular' state at 50° incidence. The normal force has small fluctuations in magnitude which are probably associated with the vortex structure, together with a general decrease in magnitude from the model tip towards the rear. It has not yet been possible to correlate the fluctuations with the vortex structure or, by implication, with the side force variation, but a general statement can be made about the mean level of the normal force. It can be seen that when there is a strong asymmetric vortex wake, the local normal force is large and when there is only a weak asymmetry, the normal force is low. This is seen in fig. 4 where near the nose in a region of strong asymmetry the normal force coefficient is around 2·0 and decreases further aft along the body until reaching the more normally associated value for crossflow drag coefficient with laminar separation of about 1·2 at the most aft measuring stations. Similarly, in fig. 7 the side force is low all along the body, indicating a symmetric wake vortex pattern, and the normal force value remains low along the entire length too. Though not so obviously noticeable in figs. 12 to 15, the results at other incidences have all confirmed this conclusion.

4.4 Additional Results

Most of the results in these tests have been well behaved and have fitted into the pattern which has emerged of a 'regular' state plus other intermediate states which have lower side forces that vary predictably along the body axial length x/d. However, there have been just a few cases which have produced unexpected results. These have occurred at one or two roll angles out of the twelve per set depending on incidence and which nose is used. Such phenomena have occurred only at high incidence (50° and above) for what would normally be considered a 'regular' case. An example is shown in fig. 18. This shows side and normal force distributions at 50° incidence and a roll angle of 330° from the datum. The distributions are obtained in two parts, half without using the dummy section and half with it. In the region x/d = 7·5 to 8·0, these readings should be the same using the two methods. Fig. 4 shows a similar test at ϕ = 0° which gives a 'regular' state and shows the usual good agreement obtained at this junction.

The ϕ = 330° result shows that the vortex development up to x/d = 7·0 has been fairly standard, but from there rearwards the pattern changes. The normal force drops and the side force increases. However, when the dummy is inserted the flow reverts back to the pattern that would usually have been expected. It is not known why this should happen, but it is probably due to some imperfection of the measurement section affecting the flow development. Obviously, when the dummy is inserted that imperfection is in a different part of the flowfield.

It is interesting to compare the pressure distributions at x/d = 8·0 for the cases with and without the dummy section in place. These are shown in fig. 19. The case with the dummy corresponds to the 'regular' state and shows laminar type separation from both sides of the body, coupled with different plateau levels after separation on the different sides. The change from one level to the other is at approximately 180° from leading body generator.

The other case with no dummy again shows laminar type separation characteristics from both sides of the body, but the succeeding plateau levels are greatly different. The side with the lowest pressure has a sudden large drop in pressure before recovering back to the higher plateau level and this change of level is not at 180° from the leading body generator but over to the side of lowest pressure.

Both distributions are probably due to a vortex flow created by the body, but are very different in nature.

Results such as this are very much the exception rather than the rule, but this is typical of these cases. It is interesting to note that if these experiments had been performed measuring only overall forces and not pressures then these results would not have been detected. It is possible to classify these results as 'regular' cases because of the general vortex development, but also to be aware that such oddities do exist and to investigate them. If only overall force measurements were available, they probably would not be classified as 'regular'.

4.5 Wool Tuft Flow Visualisation

During the past year the technique of using a wool tuft grid for flow visualisation has been successfully developed.

As little information on the appropriate design of such grids could be found, a preliminary study was performed. Four grids were made, each 12 cms square overall. The mesh sizes were 1·0 cm, 1·5 cm, 2·0 cm and 3·0 cm with wool tuft lengths the same as the mesh length. The tufts were fixed to the mesh crossover points on short lengths (about 1·0 cm) of cotton to provide a flexible joint. The grids were mounted on hand-held handles and each was tried as a means of visualising the flow in the lee of the body. By this means it was established that the optimum mesh size for this particular application was 1·5 cm. This combined reasonable resolution of flow properties with a grid not requiring too much work to construct.

A new grid was constructed as shown in fig. 3. The mesh size of 1·5 cms was used with 3·0 cm tufts secured on 1·5 cm cotton. The outside frame was 19·5 cms giving a 12 x 12 mesh except for the semicircular cut-out. This was a 2·54 cm radius cut-out made so that it would fit round the body of the model.

The grid was held in position by using two retort stands and two short metal rods, plus small screw clamps. In this manner the grid could be moved independently of the model to any desired location, and the model could be rolled without moving the grid. Fig. 3 also shows the arrangement used for photographing the flow patterns in the tuft grid. The camera was mounted at the back of the model pointing upstream towards the nose. Black paper was secured to the inside of the tunnel as a background for the white tufts and lighting was by means of three floodlights shone through the tunnel windows.

This technique proved to be very successful as a means of flow visualisation. The flow patterns produced were very strong and very steady. It was possible to see the changing flow patterns as the model was rolled. There did not appear to be any hysteresis nor any 'switching' of the pattern between flow states. As the model was rolled from one hand of the 'regular' state to the other hand the flow pattern could be seen to change too. Where the pressure measurements had shown the variation with roll to be slow, so too did the wool tuft grid. Likewise when the change was fairly rapid, particularly at the higher incidences, this was reflected in the tuft patterns.

This visual exercise showed that the technique would probably be useful, so pressure measurements were made to see what effect the presence of the grid would have. Fig. 20 compares the pressure distribution at station $x/d = 4{\cdot}0$ for the two cases of no grid present and the grid placed at $x/d = 8{\cdot}25$. At this point the effect of the grid has been negligible and the vortex flow in the lee of the body is well established. Fig. 21 shows the similar comparison, but at the station $x/d = 8{\cdot}0$, very close to the grid position. Obviously, the grid has some effect here although the distribution is of the same form. Separation is still laminar, but the pressure difference in the separated region is reduced. The pressures around the body are generally not as low, probably due to the drag of the grid slowing down the flow in its vicinity. However, the flow over the nose section and up to at least $x/d = 4{\cdot}0$ has been unaffected. This is the region which has most influence on the way the flow over the body develops, so it is likely to continue developing normally as it approaches the wool tuft grid which will reflect fairly well the pattern of the true flow.

The photographs show how well the method works. They were taken with a shutter speed which would show up the flutter of the tufts near the vortex centres (about 1/30th second). The tufts away from these positions were very steady anyway. Each shot was repeated with an interval of about 5 seconds which showed that the patterns were steady. The pictures were all taken with the model at 50° incidence.

Fig. 22 shows three shots that were taken with the model roll set to the datum position. Also shown is the variation of the side force distribution first peak with roll angle which indicates that this is a 'regular' case. The three pictures are taken for successive intervals away from the

nose. The first with the grid placed at x/d = 3·5 shows the wake being asymmetric and two vortices present. The second picture, x/d = 5·5, shows that one vortex has been shed from the body and the second is growing in strength, while in the third picture, x/d = 7·0, both have been shed from the body and are trailing in approximately the freestream direction. A third vortex, not so easily discernible, is now being fed from the body.

Fig. 23 shows six pictures which were all taken with the grid placed at x/d = 5·5. The roll angle varies by 30° between each successive shot. Also shown is the roll angle variation of the first peak in the side force distribution. This can be used to help compare the photographs. In the first two shots, $\phi = 0^{\circ}$ and 30°, the flow patterns are very similar. This is reflected in the roll angle variation which shows both to be 'regular' cases. However, at $\phi = 60^{\circ}$ the side forces are very low and this is seen to be associated with a fairly symmetric body wake. At $\phi = 90^{\circ}$ the flow is practically the mirror image of that at $\phi = 0^{\circ}$ and the measurements show this to be a 'regular' case of the opposite hand. This pattern is repeated at $\phi = 120^{\circ}$, while at $\phi = 150^{\circ}$ the pattern has reverted back to be the same as at $\phi = 0^{\circ}$. This trend is also true with the measurements showing both to be 'regular' cases of opposite hands. This agreement between measurement and flow pattern is repeated throughout the roll angle range.

Hence this is a method of flow visualisation which is very effective and very simple to use, and the results obtained can be readily understood and related to the measurements.

5. SUGGESTED TEST TECHNIQUE

The results obtained in this study have made it possible to suggest a test technique to be followed whereby variations between sets of experimental results will be reduced to a minimum. Results published in available literature have often shown lack of repeatability or poor comparison against other data. It is considered that most of these problems could be overcome by following these guidelines.

Firstly, a rigidly mounted model should be used so that no problems with model vibration are encountered. The wind tunnel facility should have low freestream turbulence. It was shown early in this investigation (refs. 5 and 6) that the level of freestream turbulence can have a significant effect on the time-averaged pressures on the model body, and that the lower the turbulence level, the less the perturbations in the pressures and hence forces experienced by the model. It has been shown by Lamont in ref. 10 that Reynolds numbers in the critical transition region should be avoided, otherwise the results are unrepeatable and meaningless. He has shown that the tests should be performed with either totally laminar or totally turbulent boundary layers at separation. The maximum side forces involved are fairly similar and the results are repeatable.

A roll angle traverse at moderately high incidence should be performed to identify the 'regular' states. With more complex models it may not be possible to roll the whole body or to obtain the overall pressure distributions as was done in these experiments. It is suggested that in such cases suitably positioned pressure tappings should be made on each side of the body, which is kept at a constant roll angle. Two pressure tappings should be symmetrically placed, one at each side of the body. The model should be made so that the nose section can be rolled independently, then by monitoring the pressure difference between the two tappings it should be possible to identify the 'regular' states.

Having identified the roll ranges for 'regular' states at the one incidence, these should then be the same for all other incidences and the rest of the testing should be done in this 'regular' state. If the nose section is modified at all the roll traverse should be repeated to again identify the regions of the 'regular' state.

In this manner data will be obtained which involve the maximum forces, can be applied universally and will bear comparison with other data. Accurate trends may then be identified concerning such parameters as Mach number, Reynolds number, nose fineness ratio, etc.

6. FUTURE TESTS

There is much work which could be done in this field now that a reliable test technique has been proposed. Data could be obtained on effects of nose bluntness and nose fineness ratio for instance. However, it is first necessary to ensure that the test technique works beyond doubt.

This work has started. Firstly, a new short body section has been constructed as shown in fig. 24. This enables the nose section to be rolled independently of the body section. The new section is $\frac{1}{2}$ body diameter in length, which means that the first measuring station is 4·0 diameters from the nose tip instead of 3·5 as before. Using this section a series of tests has been conducted in which the body was held at a constant roll orientation (0°) while the nose section was rolled successively from 0° to 330° in 30° steps. This was done for both noses. The results have not yet been processed through the computer or analysed, but it is anticipated that the variation with nose roll angle will be very similar to the variation shown when the whole model is rolled. Tests were also performed in which the nose roll orientation was kept constant (0°) while the rest of the model was rolled to various angles. The results, not yet processed, should show no variation with body roll angle. These results should confirm that the roll angle variation is dependent most strongly on the nose roll angle and it is a valid technique to roll only the nose section when identifying the 'regular' state.

Work has also started on verifying the universality of the 'regular' state. It is felt that a closer roll angle resolution is necessary for both noses, at three incidences at least, to make a true comparison of 'regular' states. The first tests have been carried out at 50° incidence for both noses covering the roll angle range 0° to 180° in 10° steps. Again, the results have not yet been processed. It may prove to be unnecessary to complete the full set of tests at such a close resolution to prove the validity of the 'universal regular' state.

With both these test programs complete, they should confirm that the test technique proposed in this report will produce useful valid results. Other work can then proceed confidently.

7. CONCLUSIONS

The aims of this investigation were to try to understand why there was so much scatter in results in the available literature on high incidence testing and to try to develop a means of producing scatter-free reproducible data. The early part of this investigation showed that free-stream turbulence can have a significant effect on time-averaged pressures and forces which may be partly the cause of discrepancies in experimental results. It has also been found that roll angle has a significant effect on the flow and can completely change the forces on the body. This is probably a major cause of differences in early experimental results.

However, it has been shown that there exists a 'regular' state for the flow which may be of either hand. This state involves the maximum local side forces and normal forces. The side force is cyclic in nature, being associated with the asymmetric vortex development in the lee of the body. The strongest side forces are produced in the first half cycle, from the initially asymmetric vortices, and the forces in each successive half cycle decrease in strength. The normal force varies as the flow field changes, but not so strongly as the side force. The stronger the asymmetric vortex flowfield, the greater the normal force. At large distances from the nose tip the flow reverts to the time-dependent flow over an infinite yawed cylinder and the average normal force becomes the crossflow drag coefficient usually associated with such flows. At high incidence, over about 75°, this is also the case over the whole body. At low incidence, around 35°, the side forces are low and by implication the vortex flowfield has weaker asymmetry which produces lower normal force.

It has not been shown exactly why the flow is dependent on roll angle, but it is believed to be associated with the imperfections contained in the tip region of the nose which may be affecting the stability of the initially symmetric vortex pair formed in this region.

A technique has been proposed whereby reliable data may be obtained which will be reproducible and scatter-free.

A method of flow visualisation in the lee of the body involving a wool tuft grid has been utilised, which produces easily understood results and is simple to use.

8. REFERENCES

1. Ericsson, L.E.
   Reding, J.P.
   Vortex-induced asymmetric loads in 2-D and 3-D flows
   AIAA Paper 80-0181 1980

2. Wardlaw, A.B.
   Morrison, A.M.
   Induced side forces at high angles of attack
   J.Spacecraft, Vol.13, No.10, pp.589-593 1976

3. Lamont, P.J.
   Hunt, B.L.
   Pressure and force distributions on a sharp-nosed circular cylinder at large angles of inclination to a uniform subsonic stream
   J.Fluid Mechanics, Vol.76, Part 3, pp.519-559 1976

4. Lamont, P.J.
   Hunt, B.L.
   Prediction of aerodynamic out-of-plane forces on ogive-nosed circular cylinders.
   J.Spacecraft, Vol.14, No.1, pp.38-44 1977

5. Hunt, B.L.
   Dexter, P.C.
   Pressures on a slender axisymmetric body at high angle of attack in a very low turbulence level air stream. First Annual Report
   Univ. of Bristol, Aero.Eng.Dept. BLH/7801 1978

6. Hunt, B.L.
   Dexter, P.C.
   Pressures on a slender axisymmetric body at high angle of attack in a very low turbulence level air stream. Second Annual Report
   Univ. of Bristol, Aero.Eng.Dept. 1979

7. Clark, W.
   Body vortex formation on missiles in incompressible flows.
   AIAA paper 77-1154 1977

8. Reding, J.P.
   Ericsson, L.E.
   Maximum vortex-induced side forces on slender bodies
   AIAA paper 77-1155 1977

9. Clarkson, M.H.
   Malcolm, G.N.
   Chapman, G.T.
   A subsonic, high angle-of-attack flow investigation at several Reynolds numbers.
   AIAA, Vol. 16, No. 1, pp.53-60 1978

10. Lamont, P.J.
    Pressure distributions on an ogive-cylinder at high angles of attack with laminar, transitional or turbulent separation.
    Summary of 6th Working Group meeting on high angle of attack missile aerodynamics
    AEDC 1979

9. NOTATION

C_n	sectional normal force coefficient
C_{p_x}	pressure coefficient
C_y	sectional side force coefficient
d	body diameter
Re	Reynolds number
U	freestream velocity
x	axial distance from nose tip
α	incidence angle in degrees
θ	angular distance from freestream body generator in degrees
ϕ	roll angle in degrees
ν	kinematic viscosity

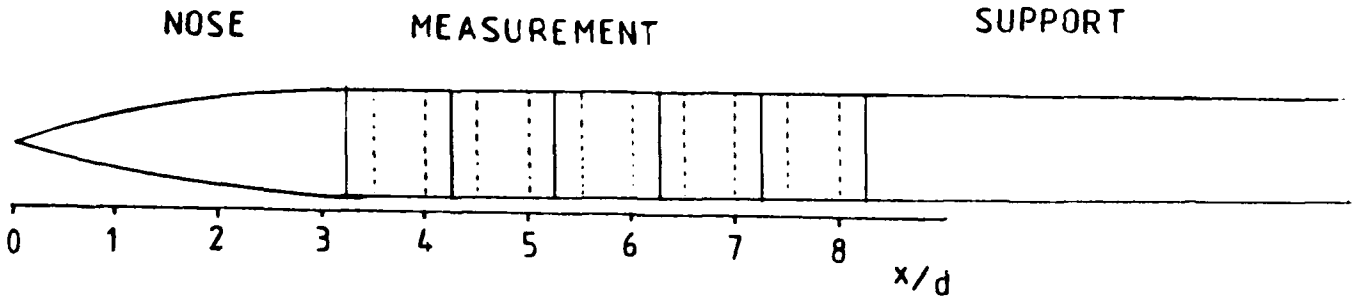

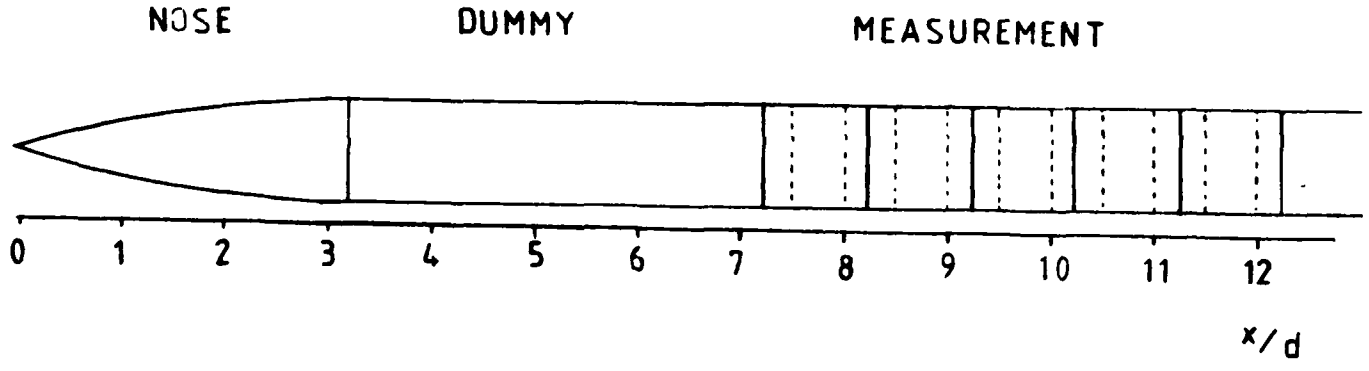

FIG 1 MULTI-PRESSURE TAPPED MODEL

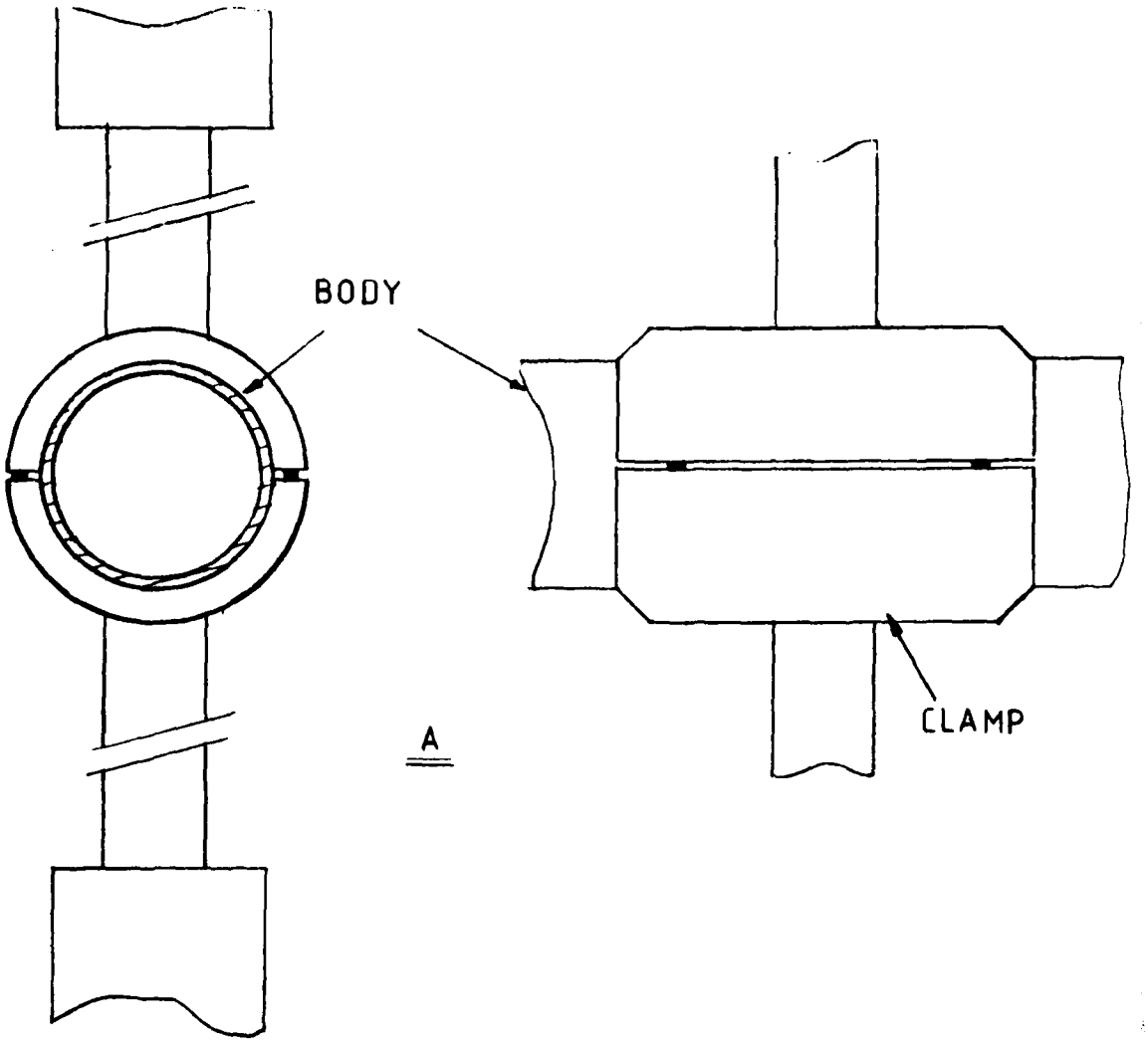

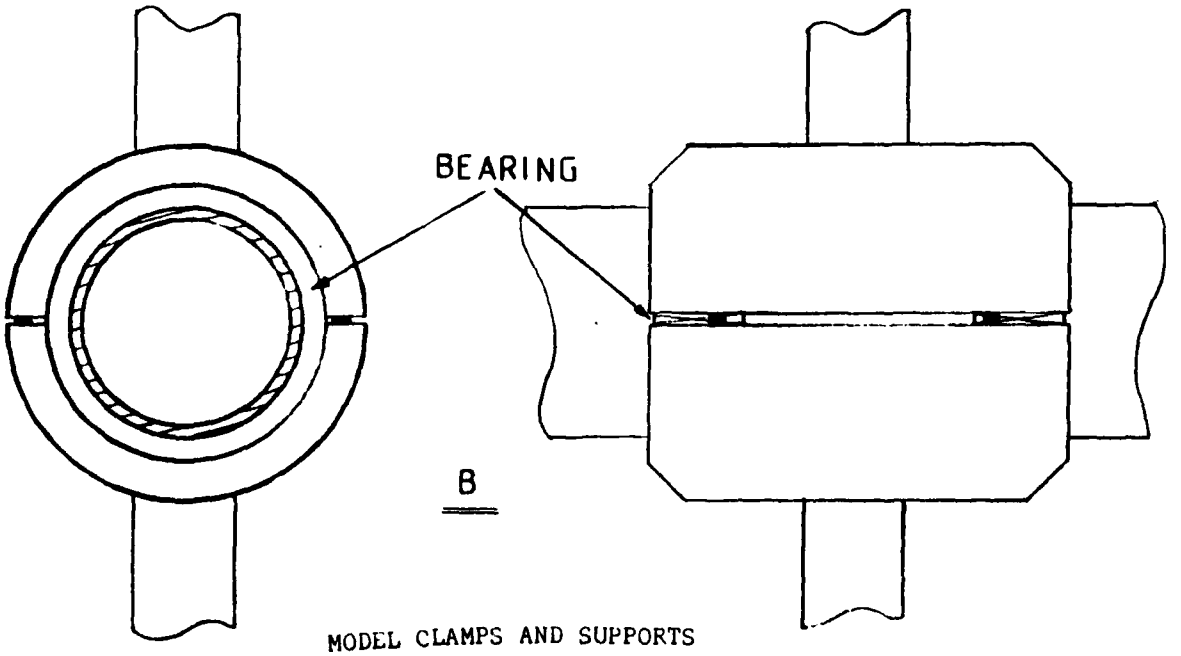

FIG 2

MODEL CLAMPS AND SUPPORTS

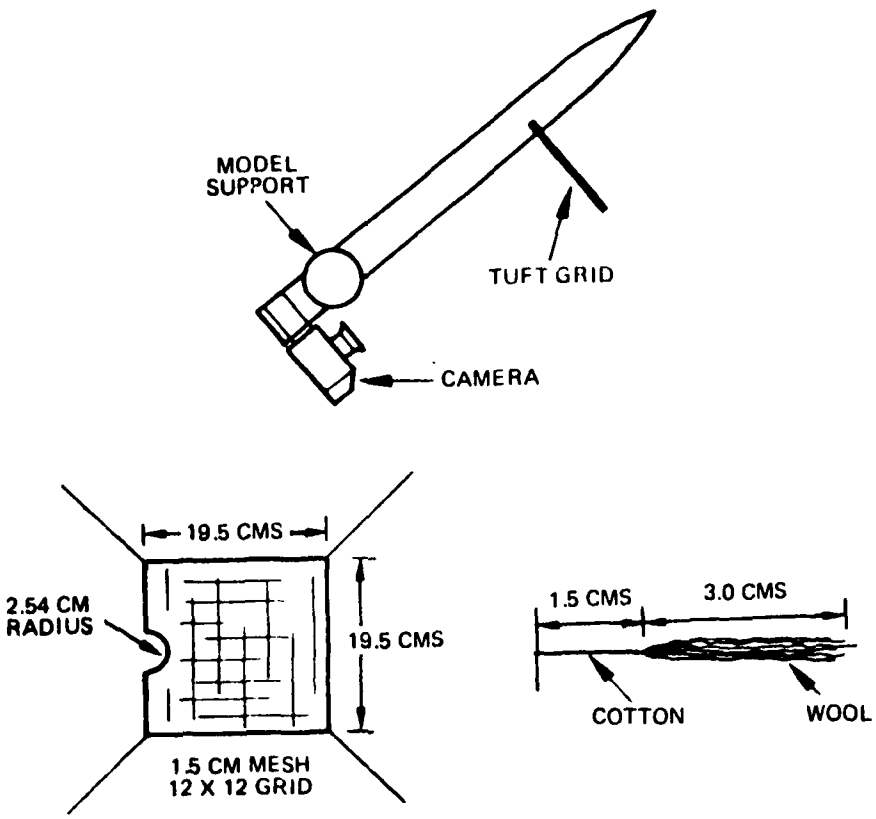

FIG 3 WOOL TUFT GRID ARRANGEMENT

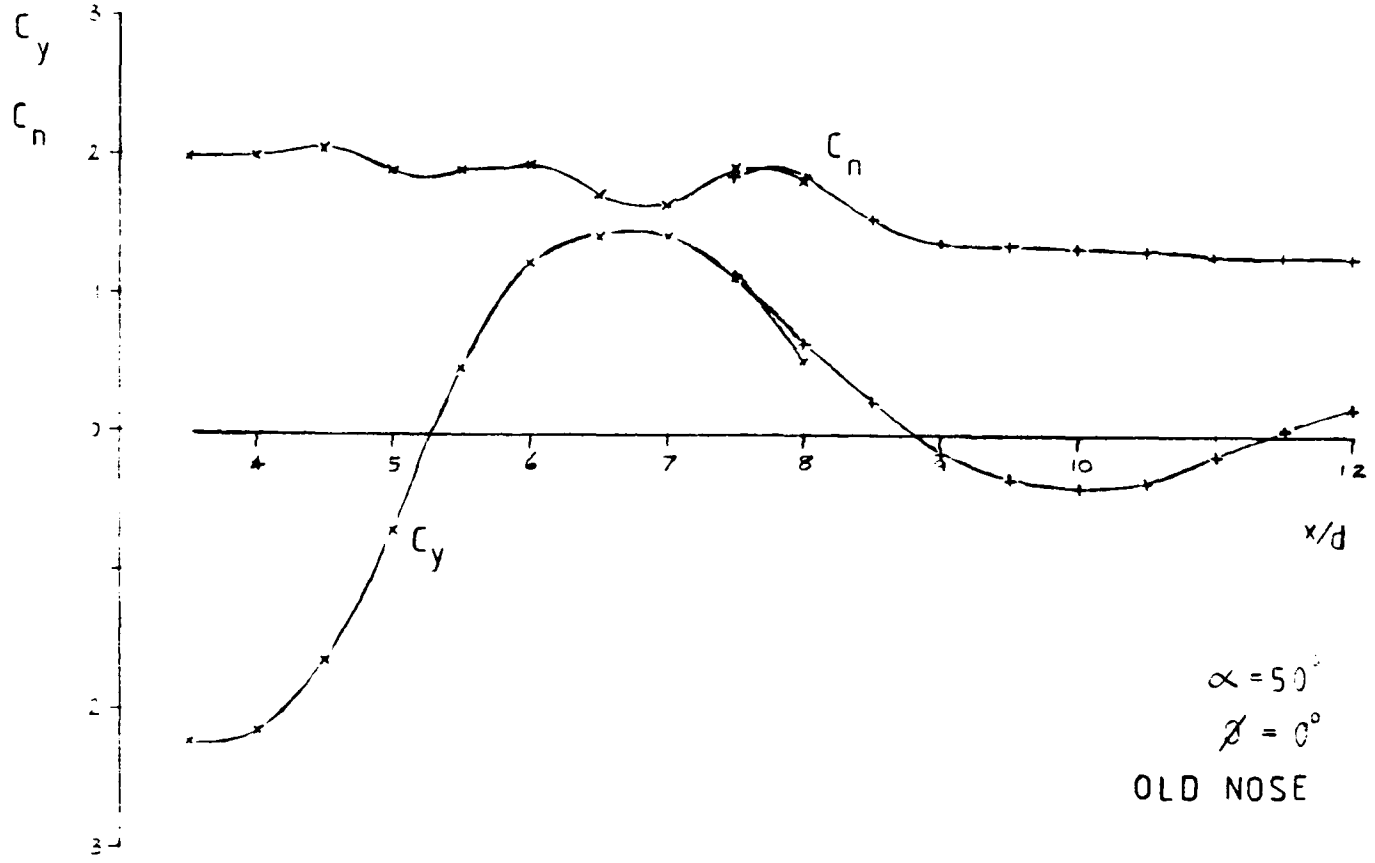

FIG 4 LOCAL SIDE AND NORMAL FORCE DISTRIBUTIONS

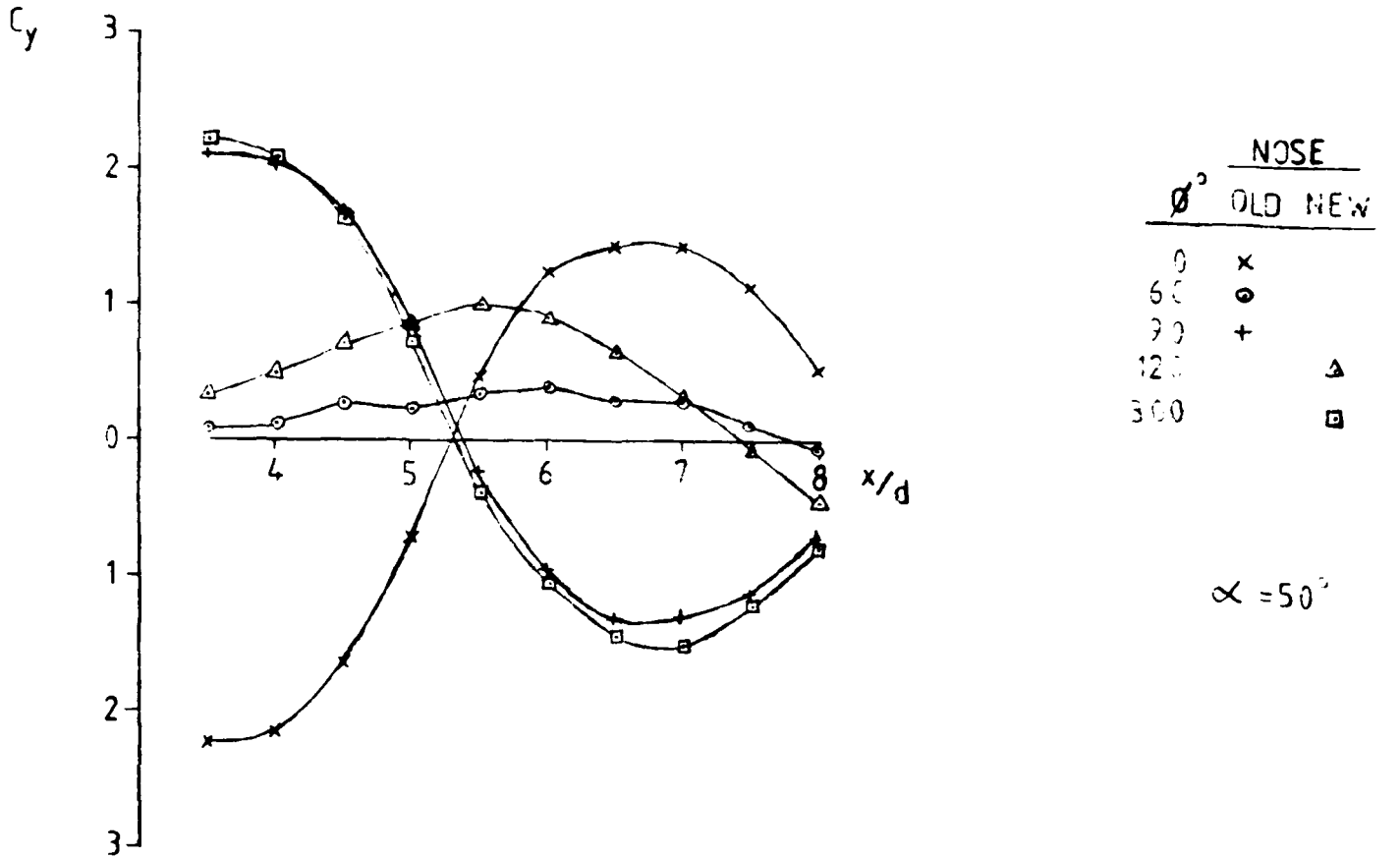

FIG 5 TYPICAL LOCAL SIDE FORCE DISTRIBUTIONS

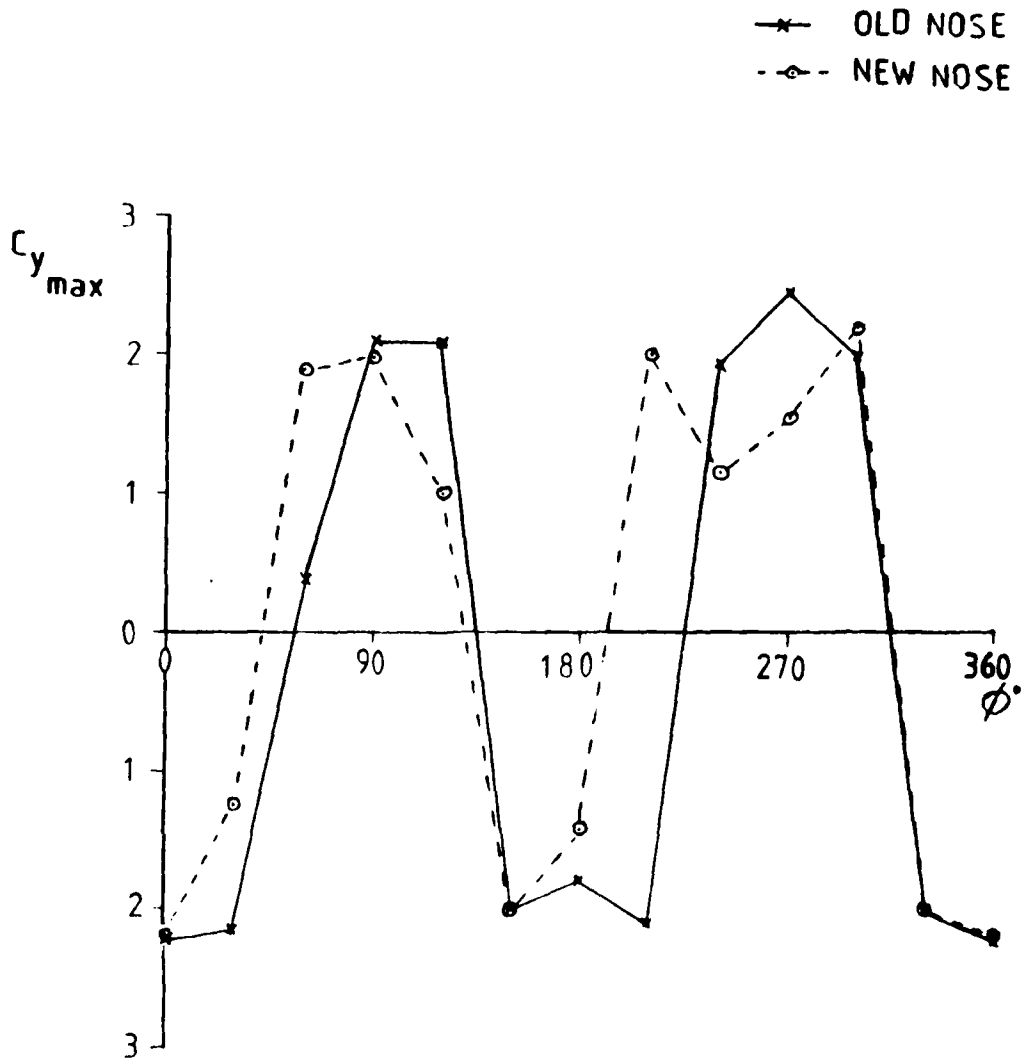

FIG 6 SIDE FORCE VARIATION WITH ROLL ANGLE

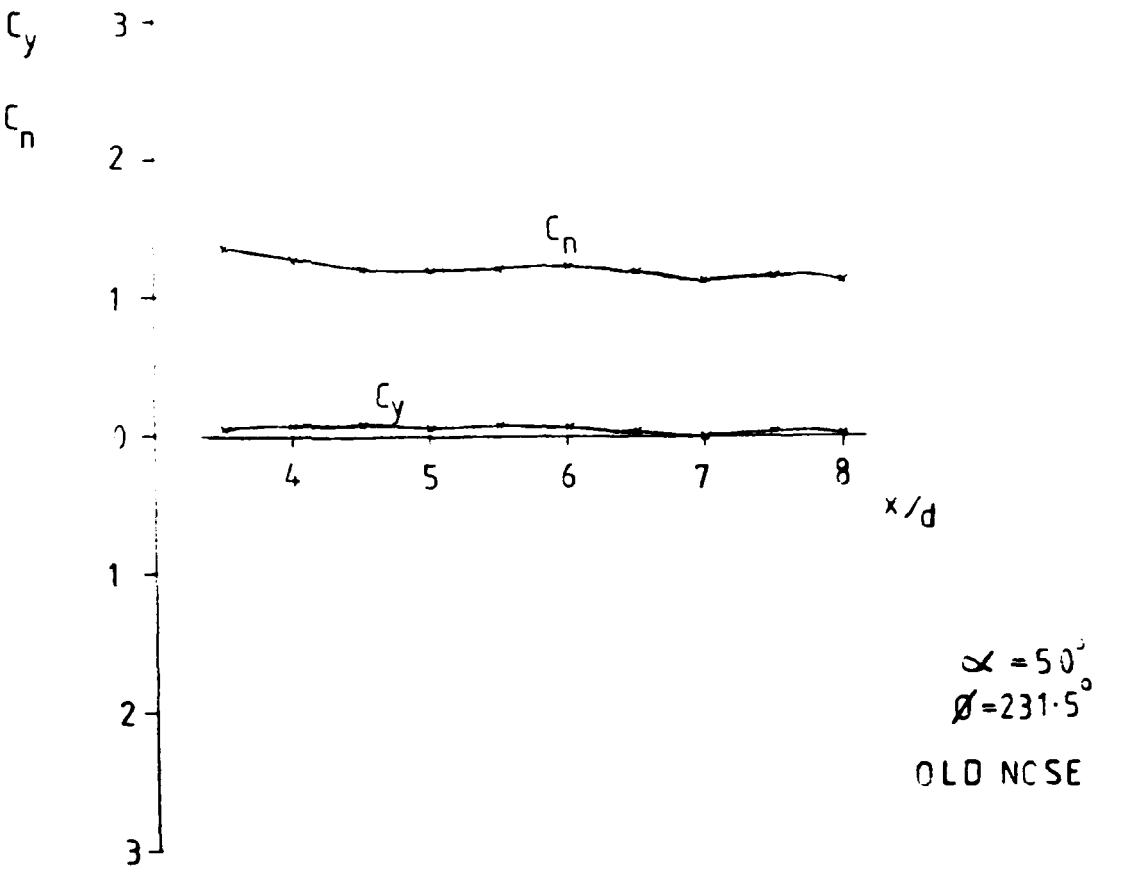

FIG 7 LOCAL SIDE AND NORMAL FORCE DISTRIBUTION

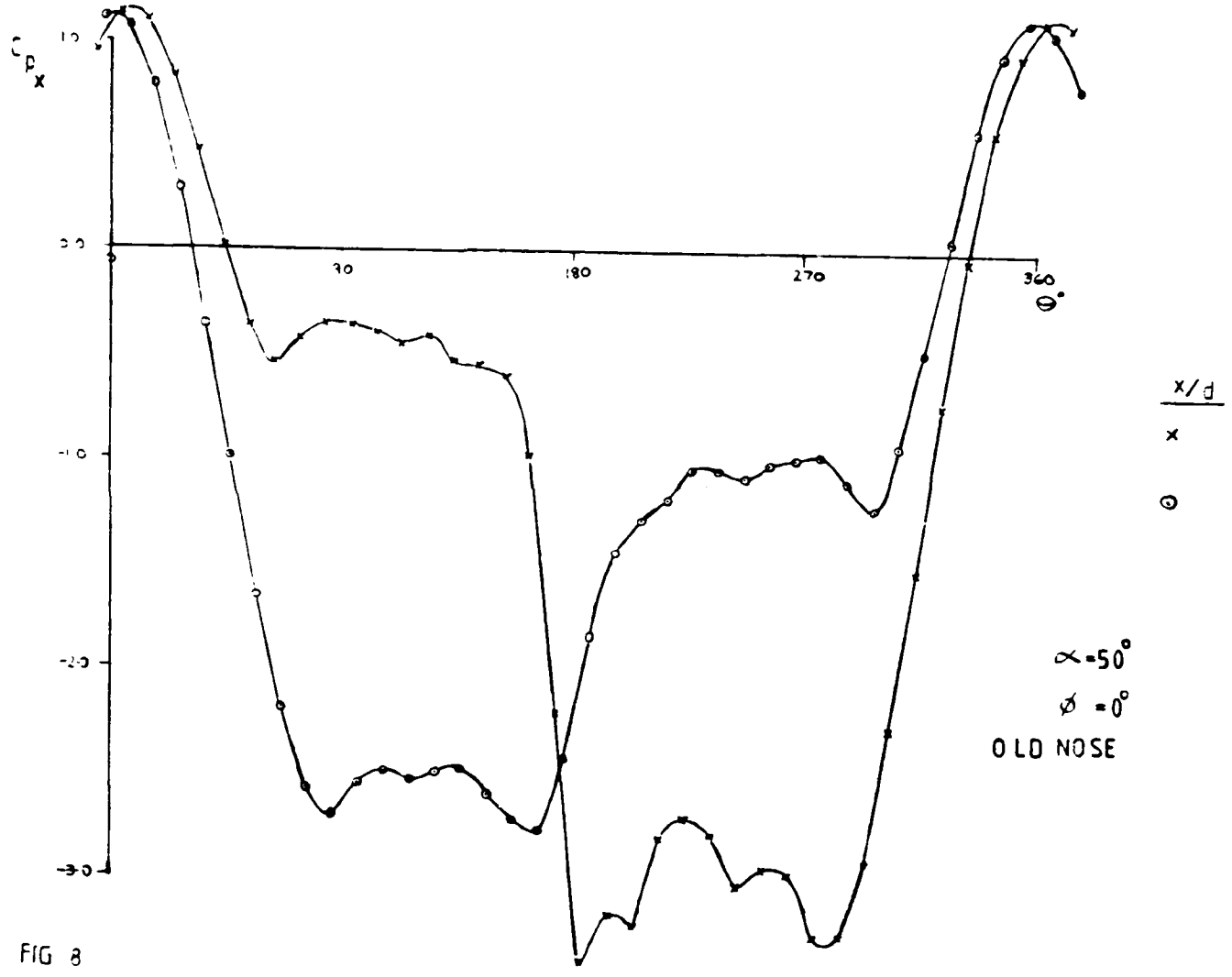

FIG 8

PRESSURE DISTRIBUTIONS FOR A 'REGULAR' CASE

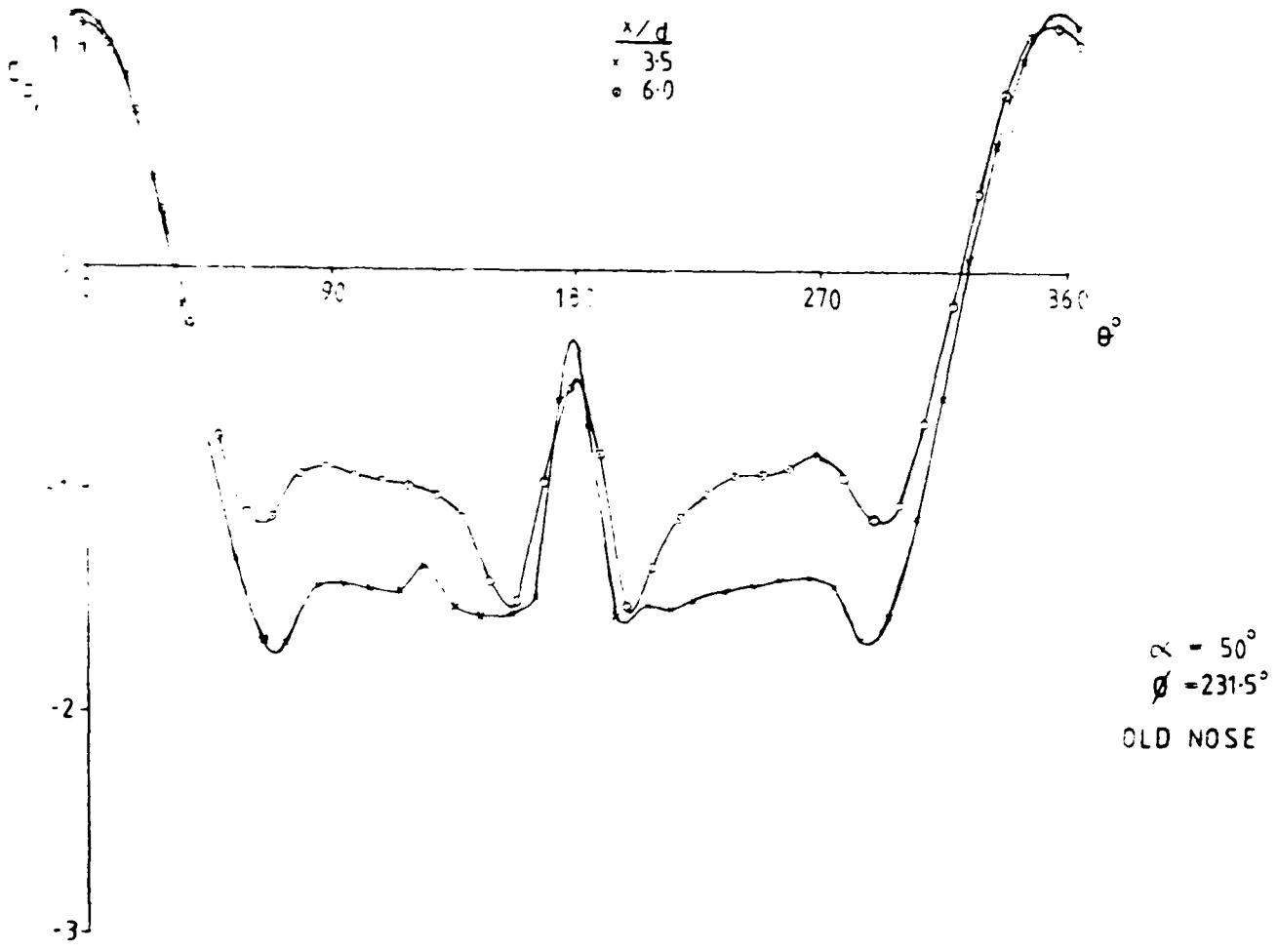

FIG 9 PRESSURE DISTRIBUTIONS FOR A LOW SIDE FORCE CASE

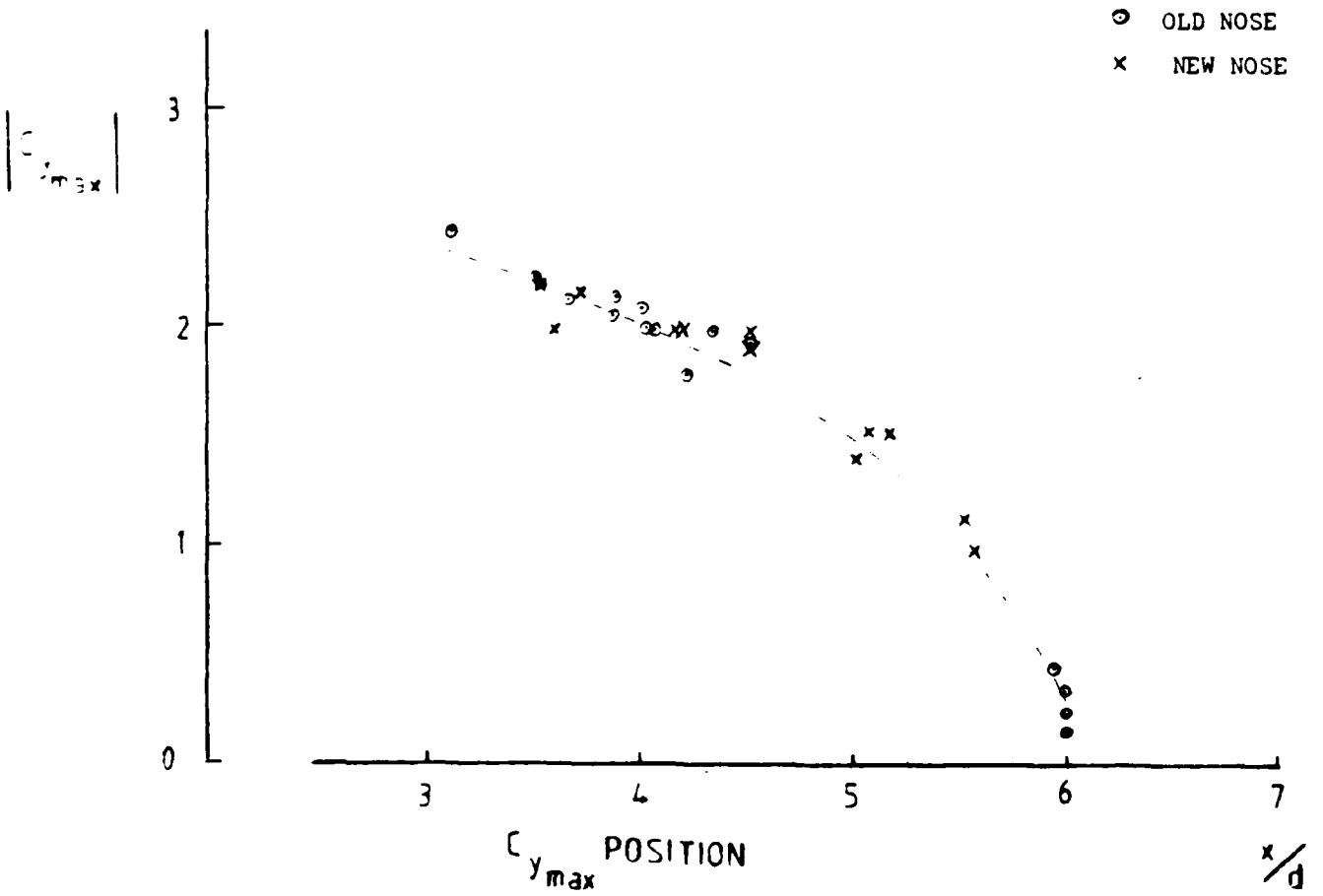

$\alpha = 50^{\circ}$ $Re = 10^{5}$

FIG 10

MAGNITUDE OF $C_{y_{max}}$ VERSUS ITS AXIAL LOCATION

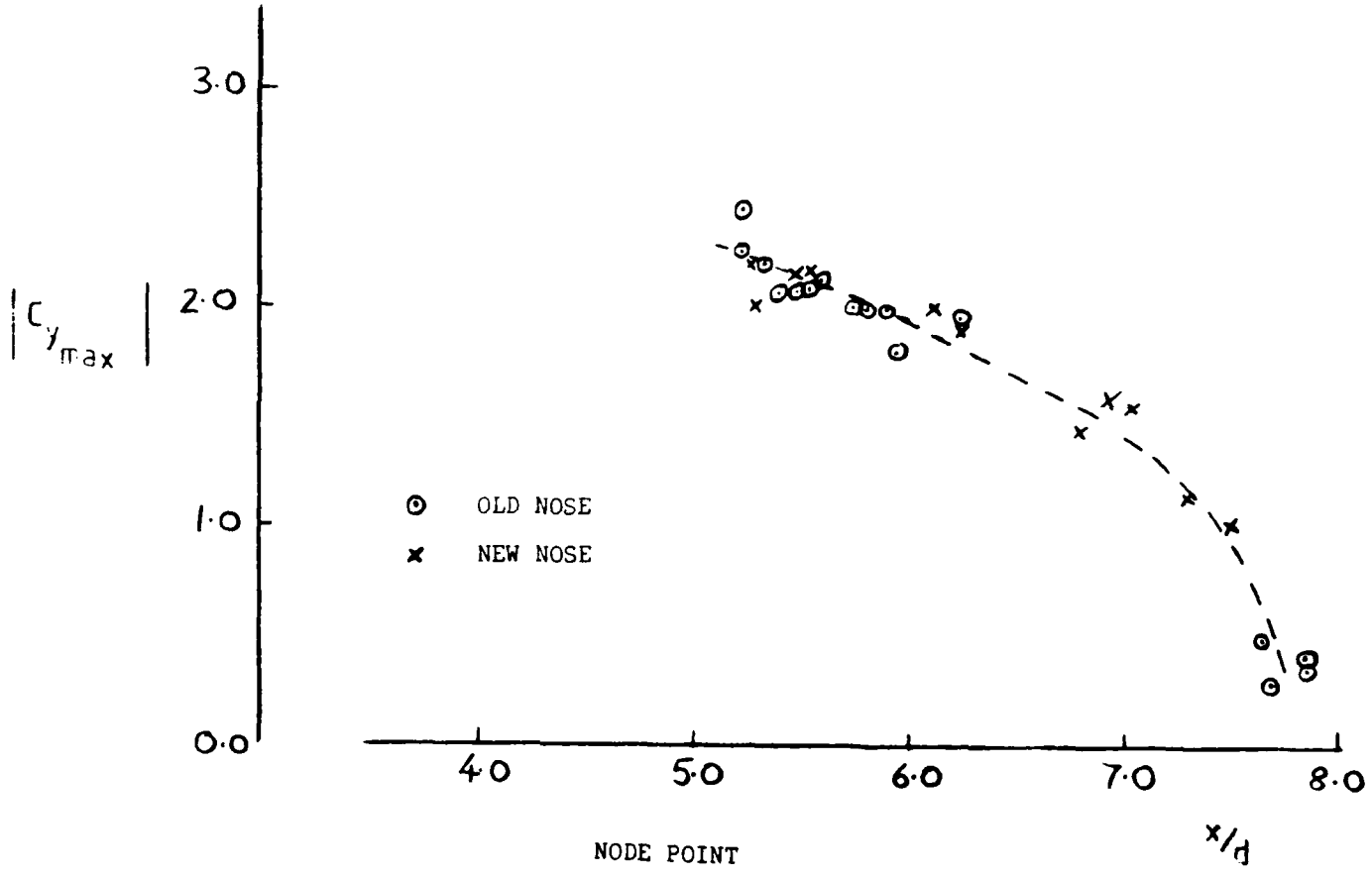

$\alpha = 50^{\circ}$ $Re = 10^{5}$

FIG 11

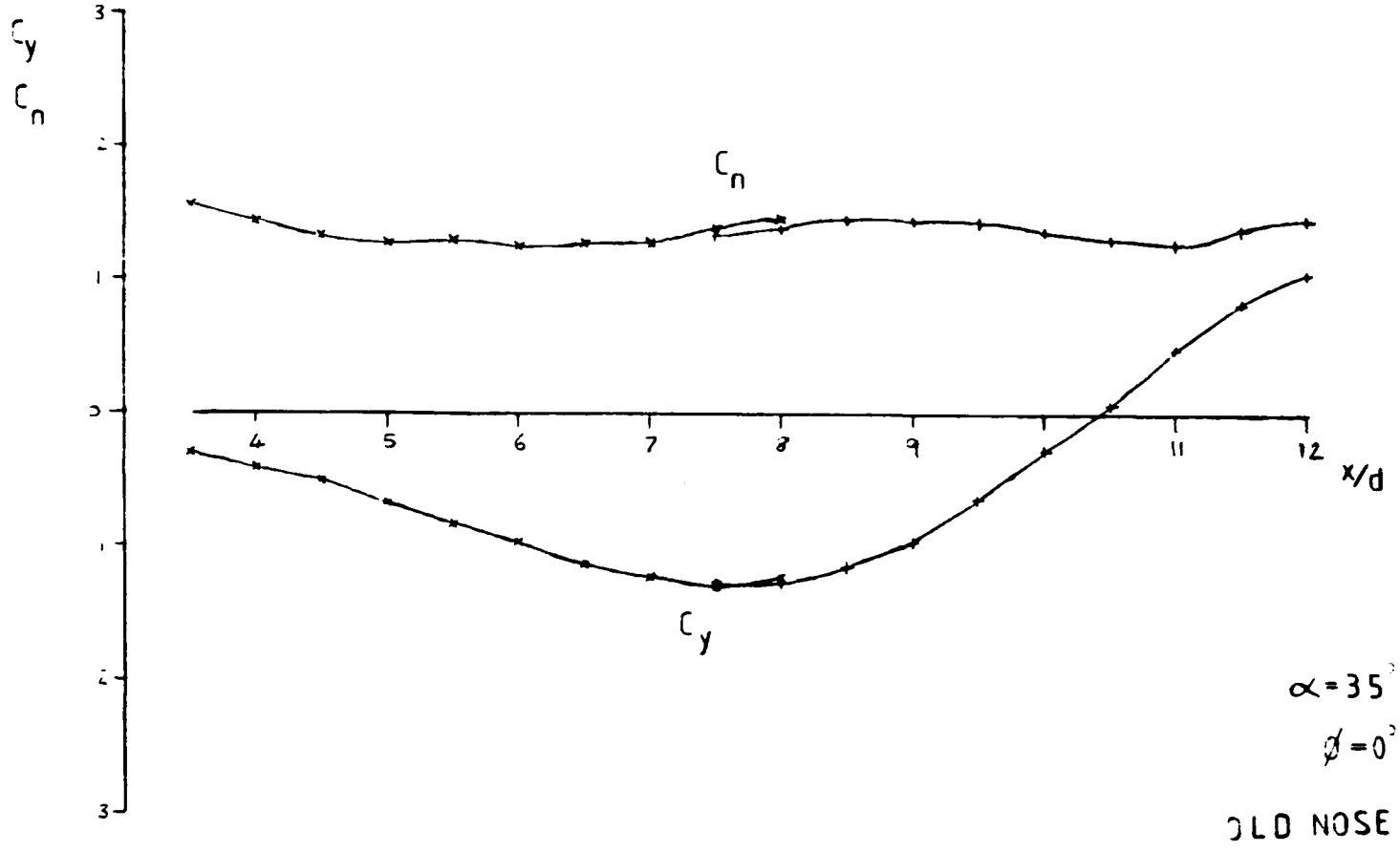

FIG 12 TYPICAL LOCAL FORCE DISTRIBUTION

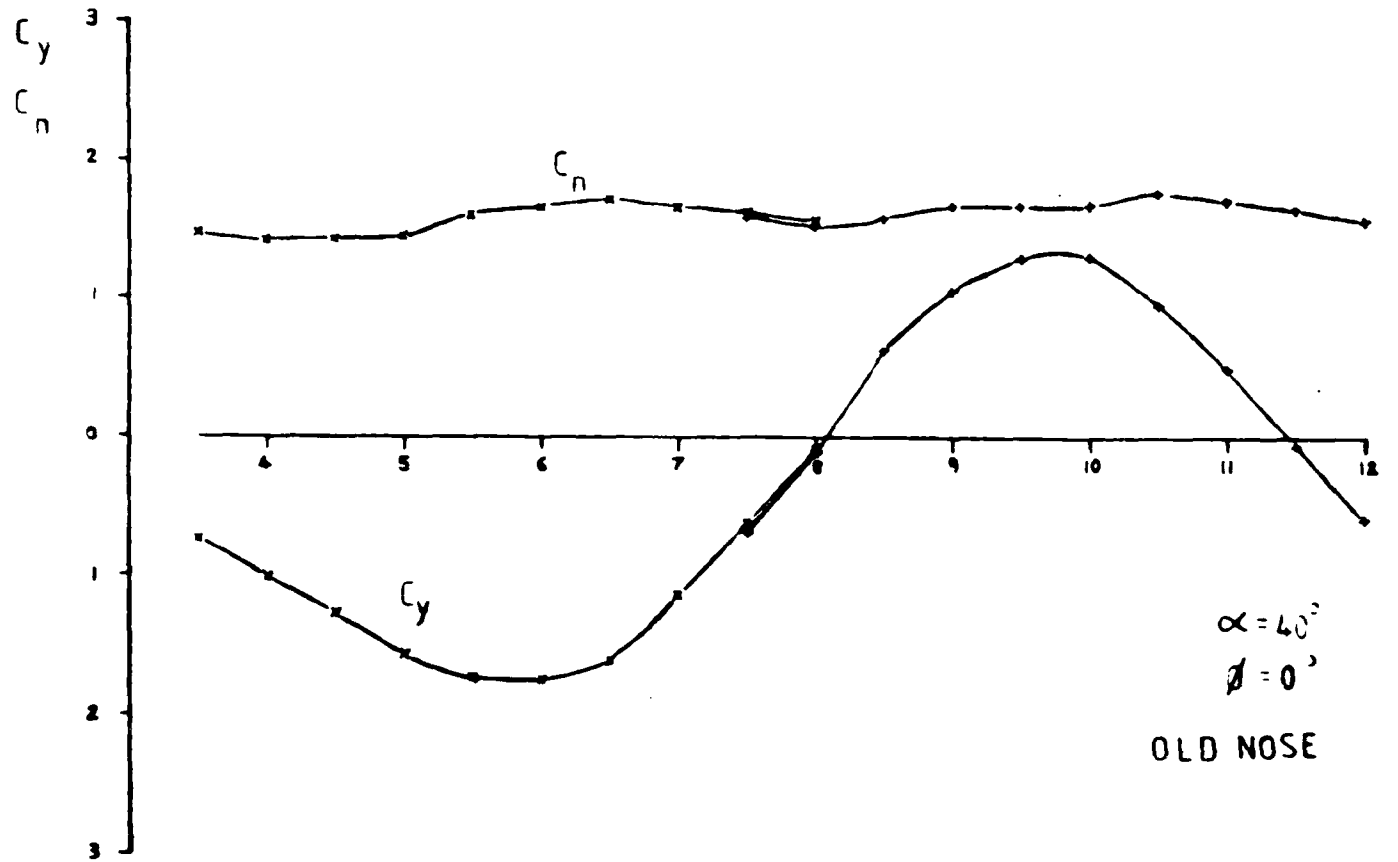

FIG 13 LOCAL SIDE AND NORMAL FORCE DISTRIBUTIONS

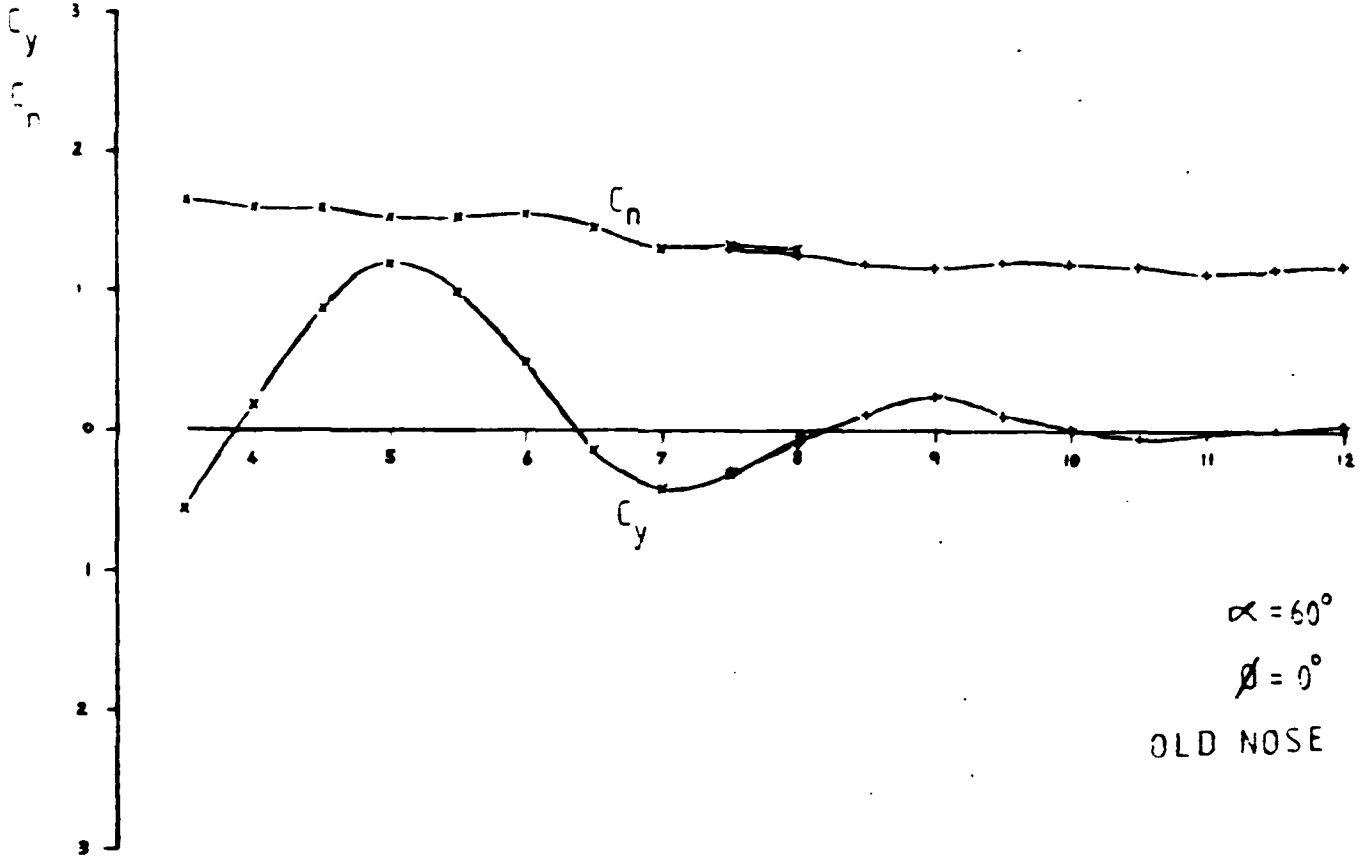

FIG 14 LOCAL SIDE AND NORMAL FORCE DISTRIBUTIONS

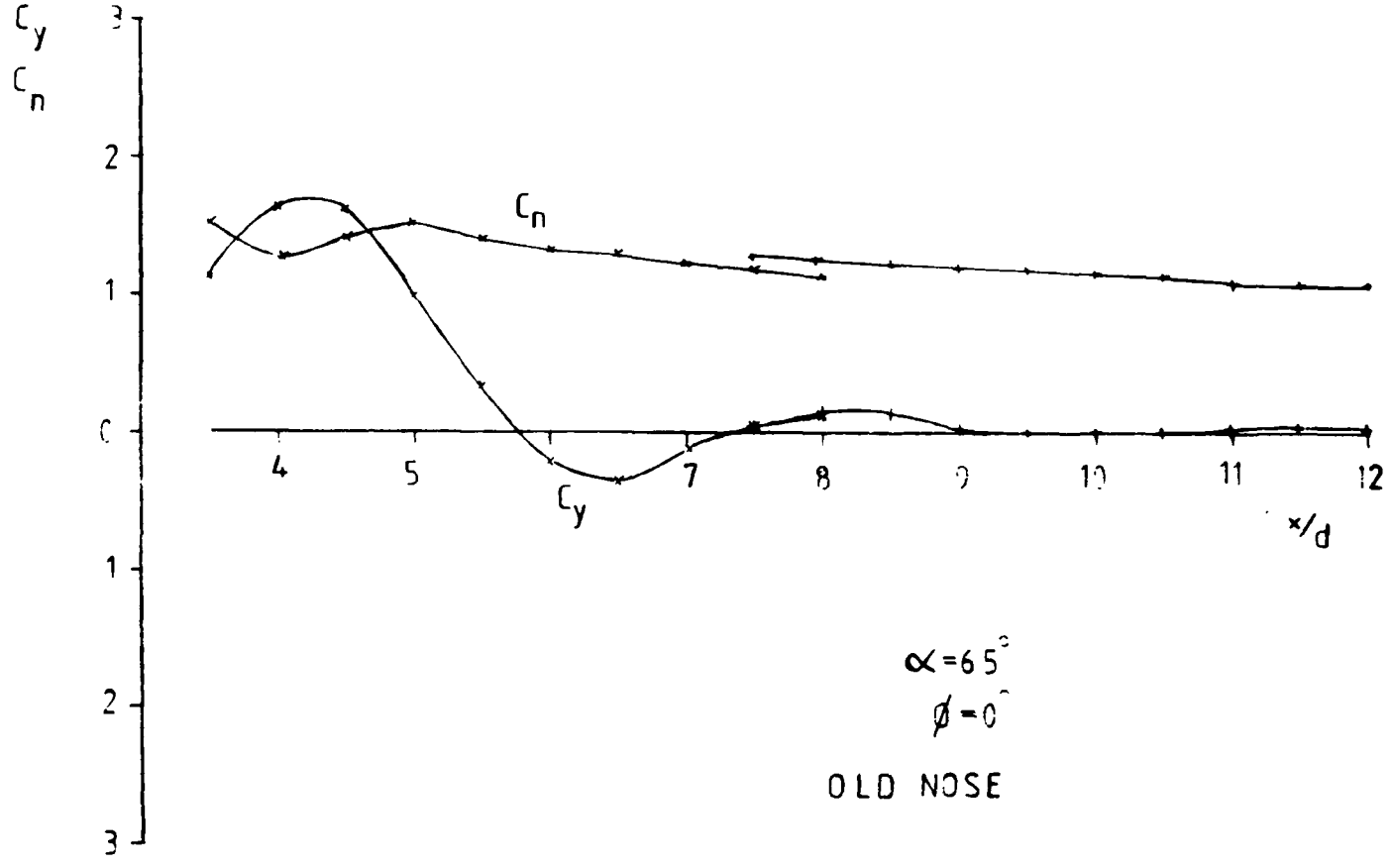

FIG 15 TYPICAL LOCAL FORCE DISTRIBUTION

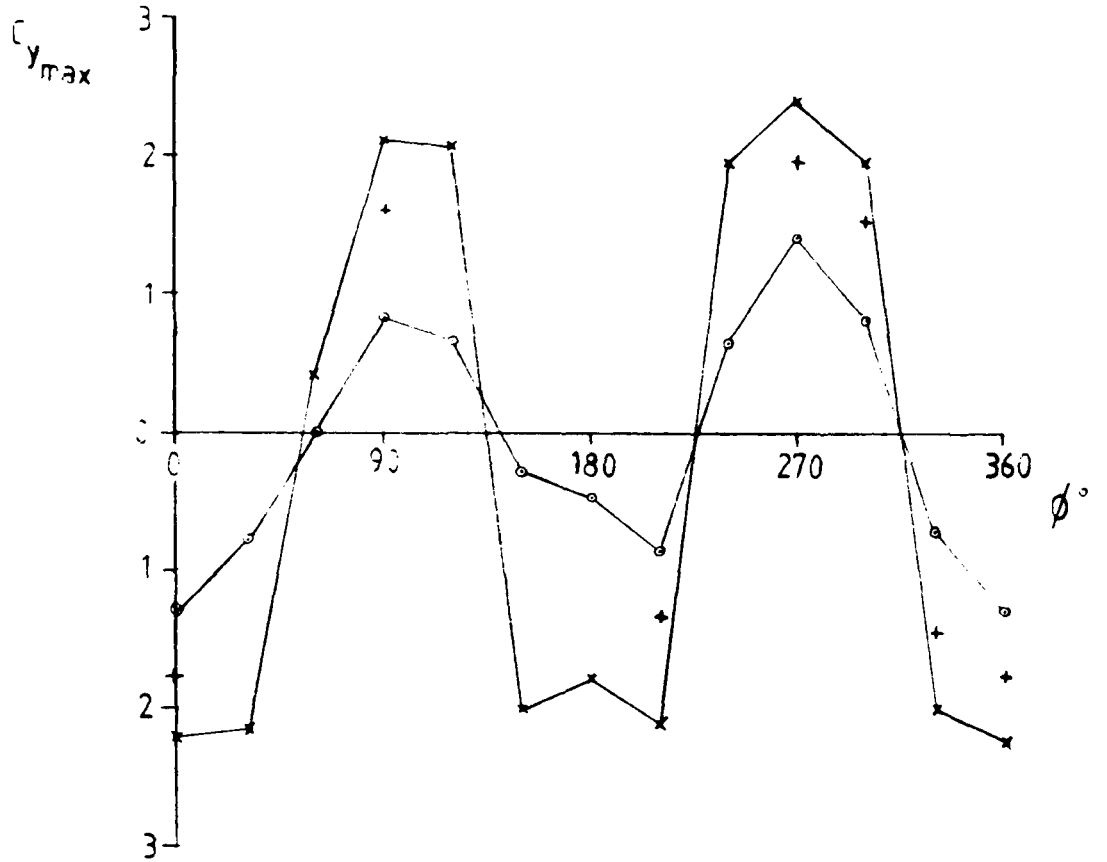

FIG 16 ROLL ANGLE VARIATION FIRST HALF CYCLE

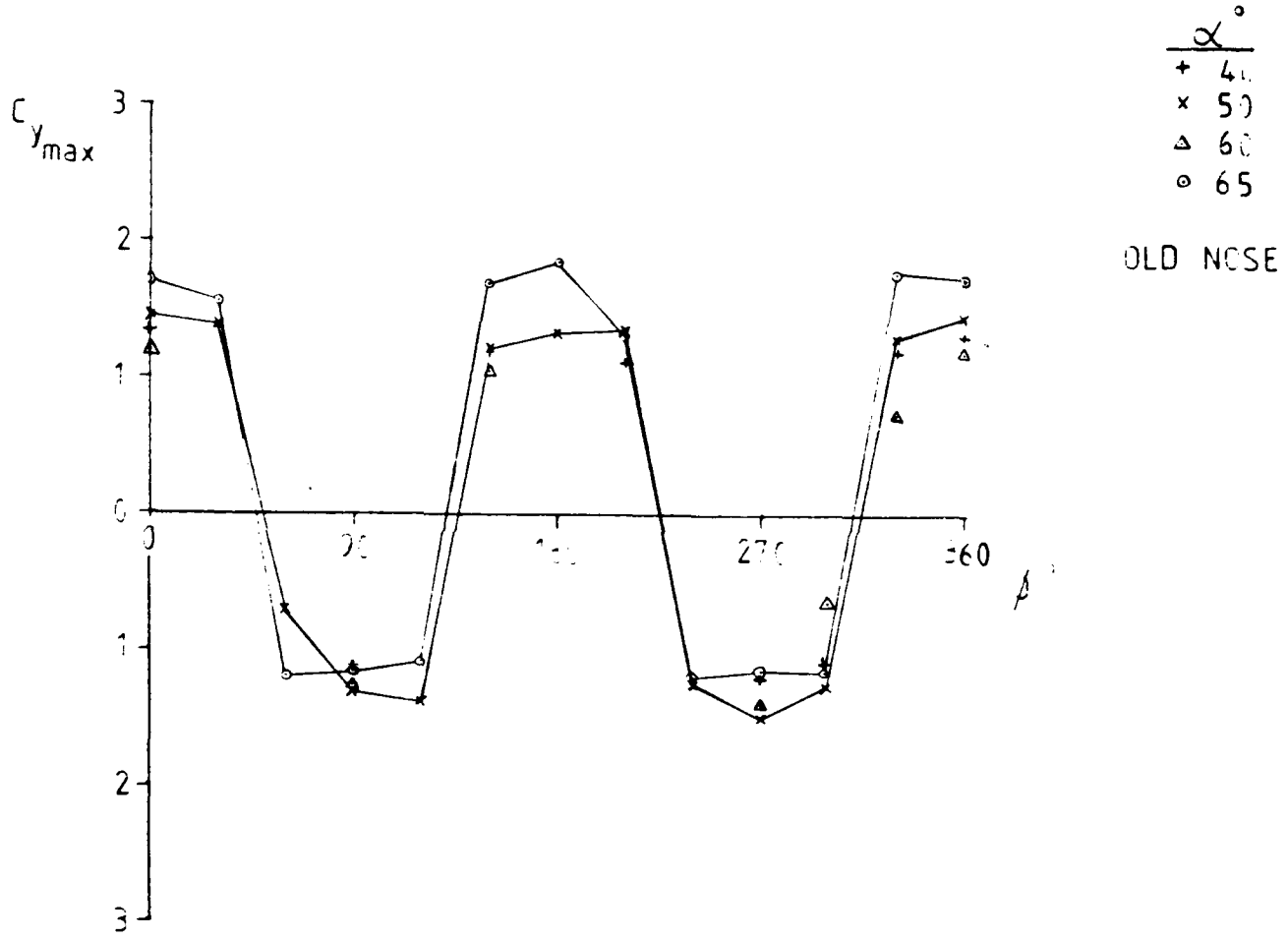

FIG 17 ROLL ANGLE VARIATION SECOND HALF CYCLE

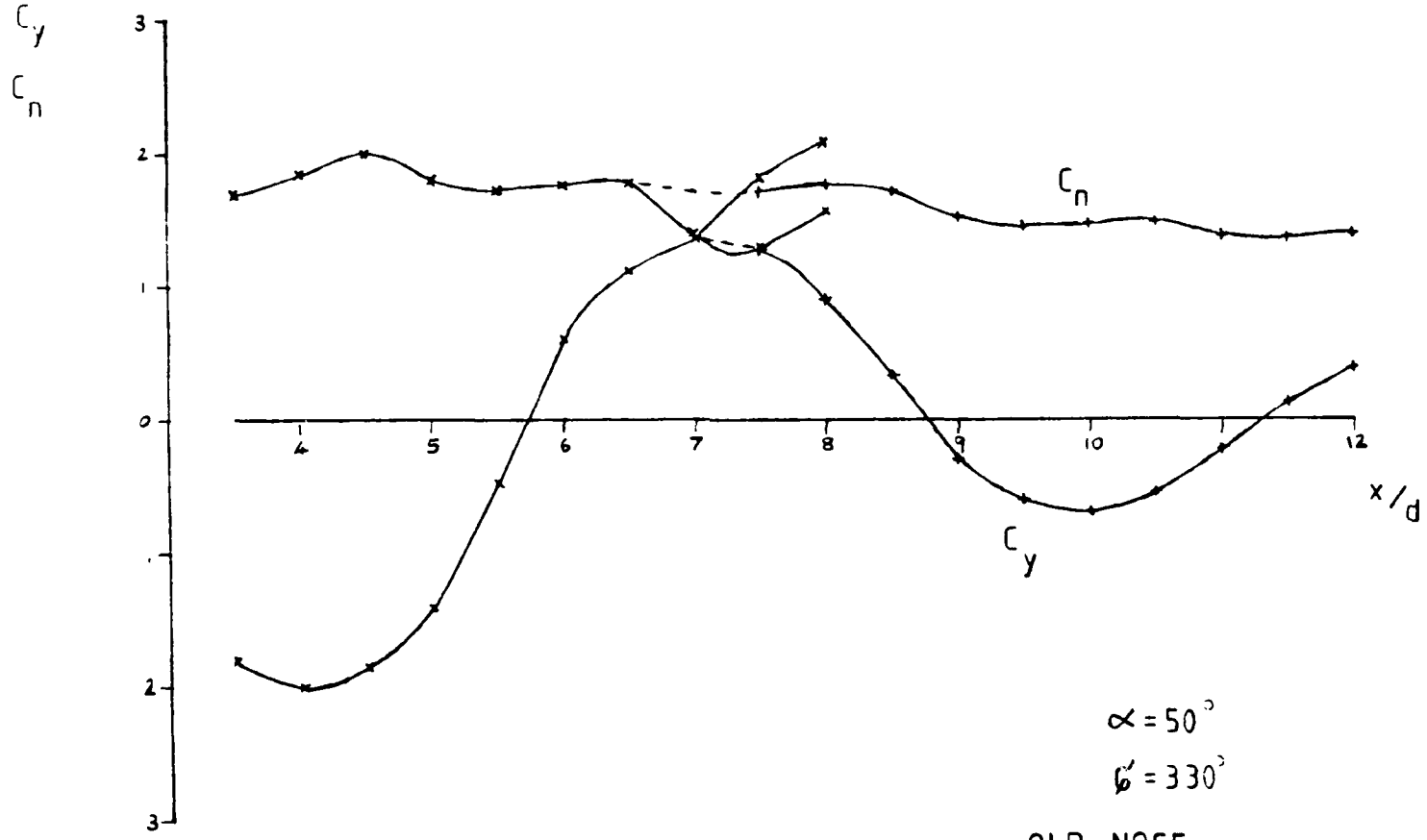

FIG 13 LOCAL NORMAL AND SIDE FORCE DISTRIBUTION

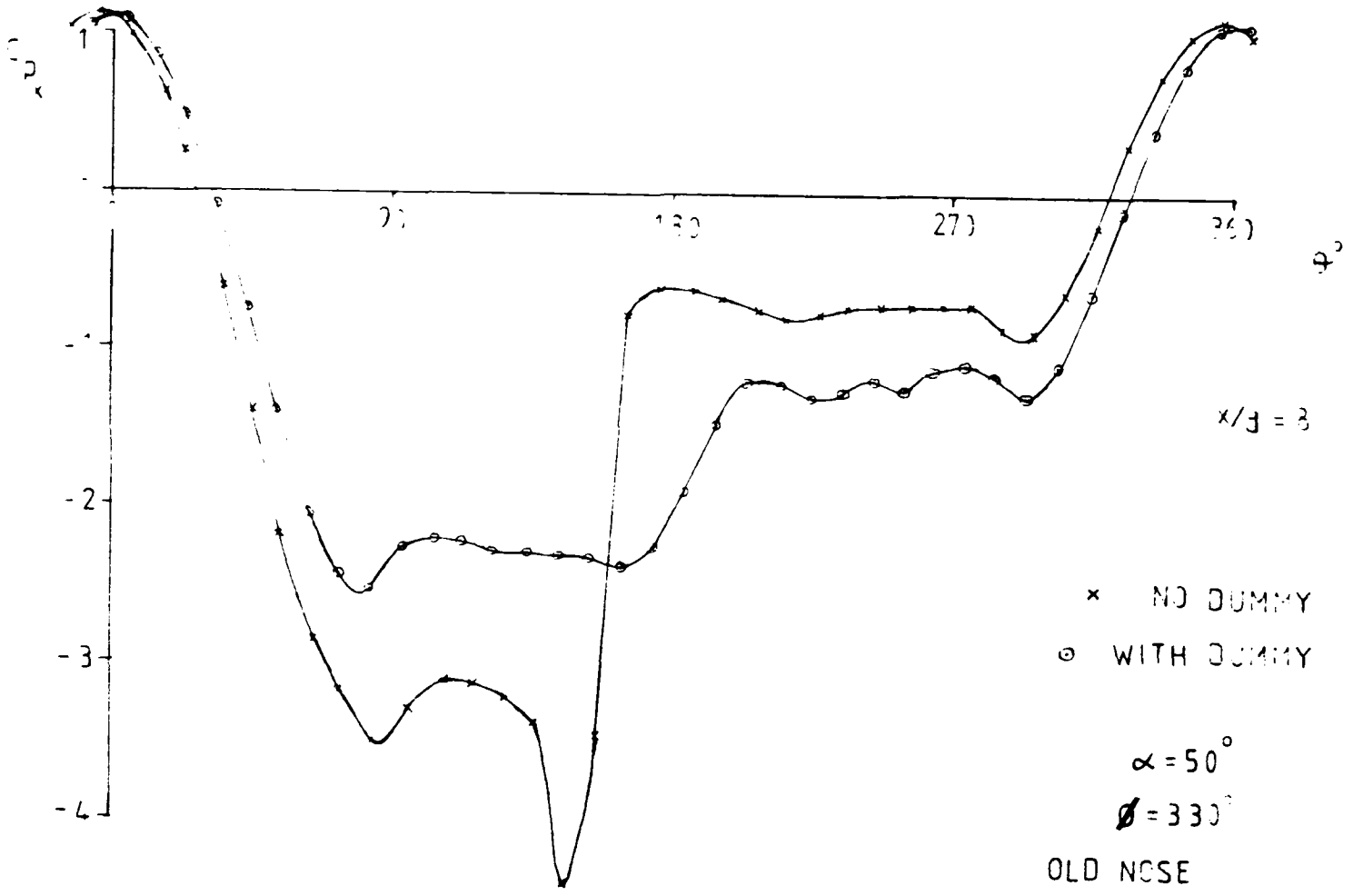

FIG 19 COMPARISON OF PRESSURE DISTRIBUTIONS

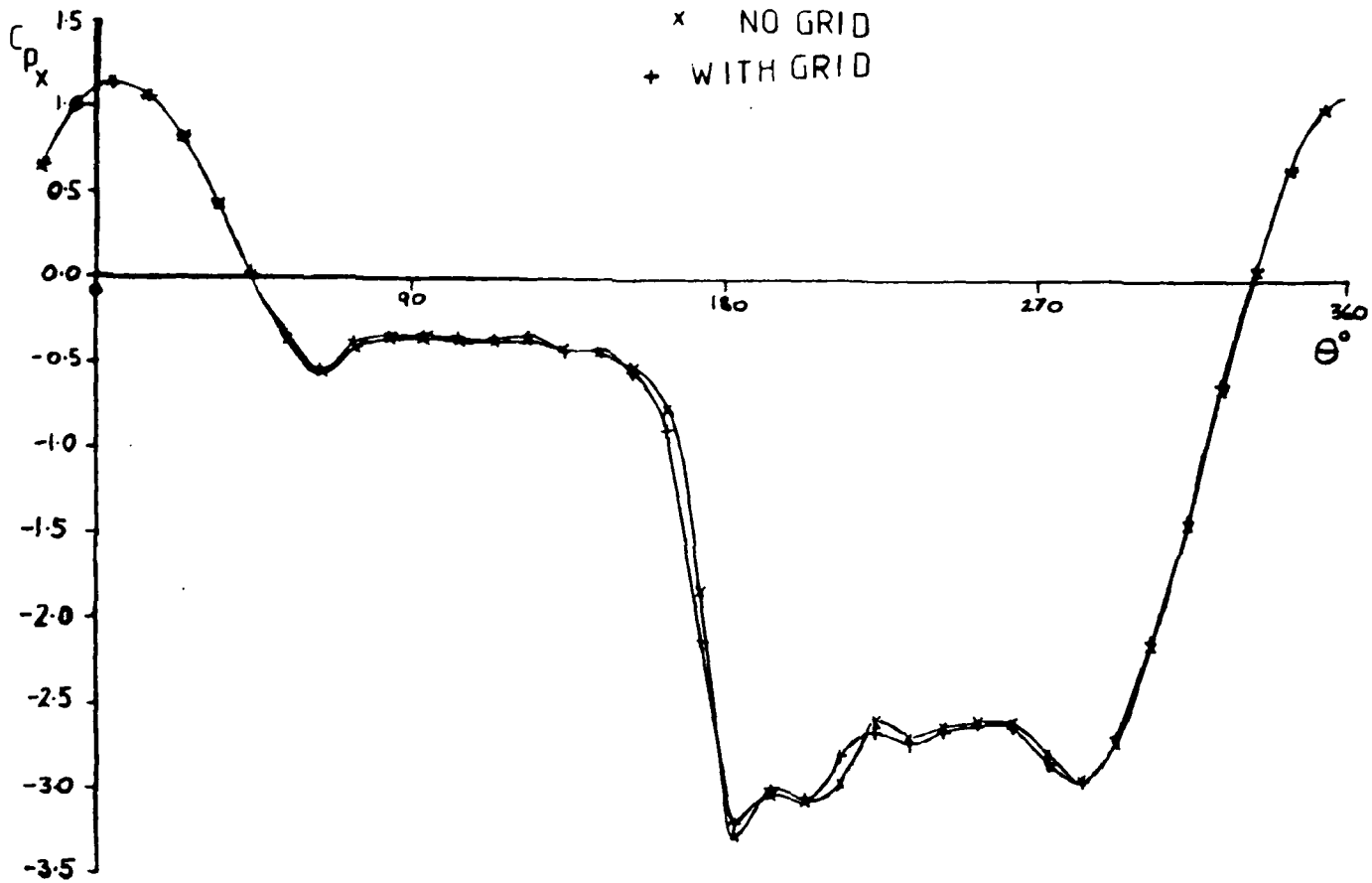

WOOL TUFT GRID PLACED AT $^{x}/_{d}$ = 8.25

$^{x}/d = 4$

FIG 20 EFFECT OF WOOL TUFT GRID ON PRESSURE DISTRIBUTION

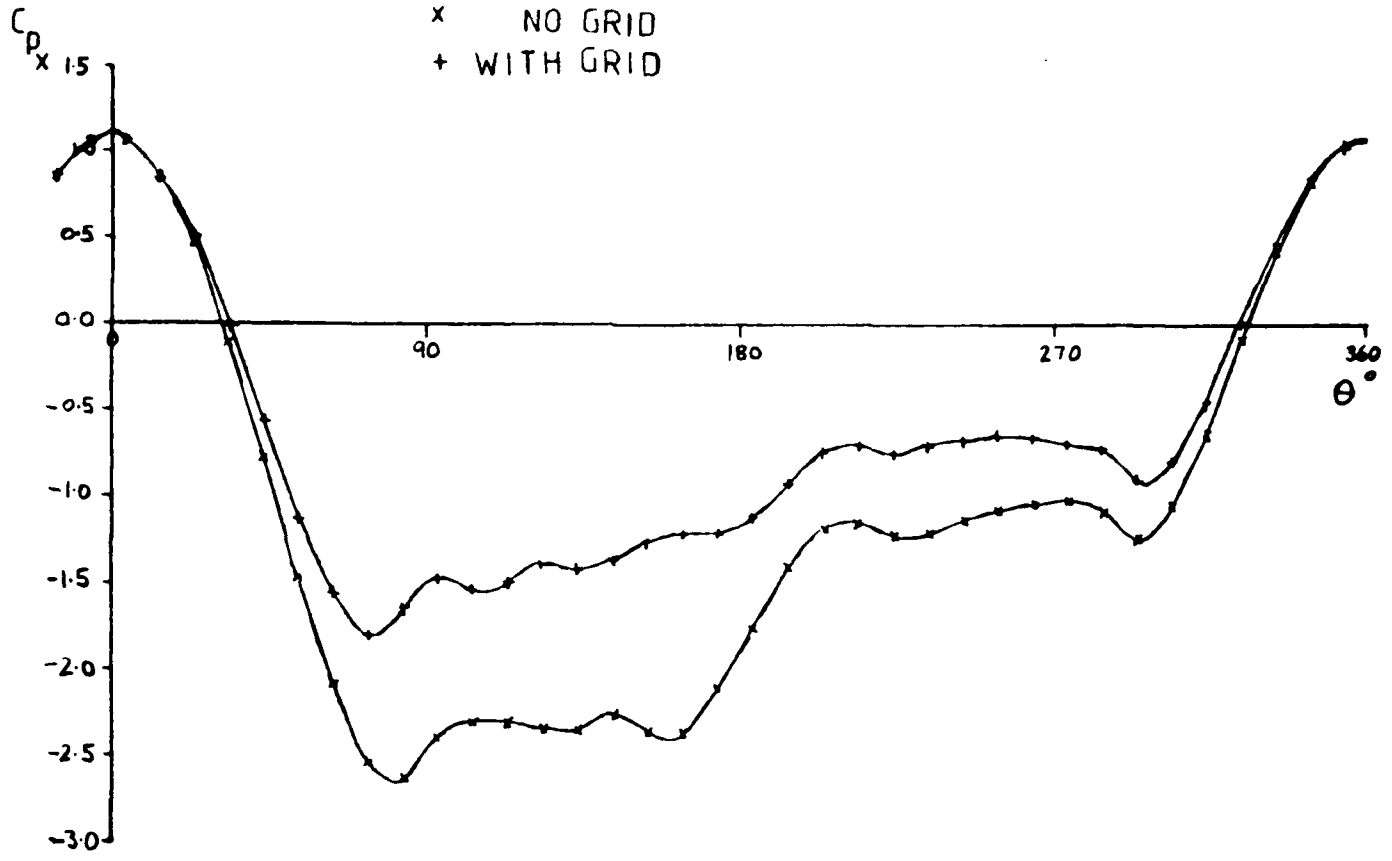

WOOL TUFT GRID PLACED AT x/d = 8.25

$x/d = 8$

FIG 21 EFFECT OF WOOL TUFT GRID ON PRESSURE DISTRIBUTION

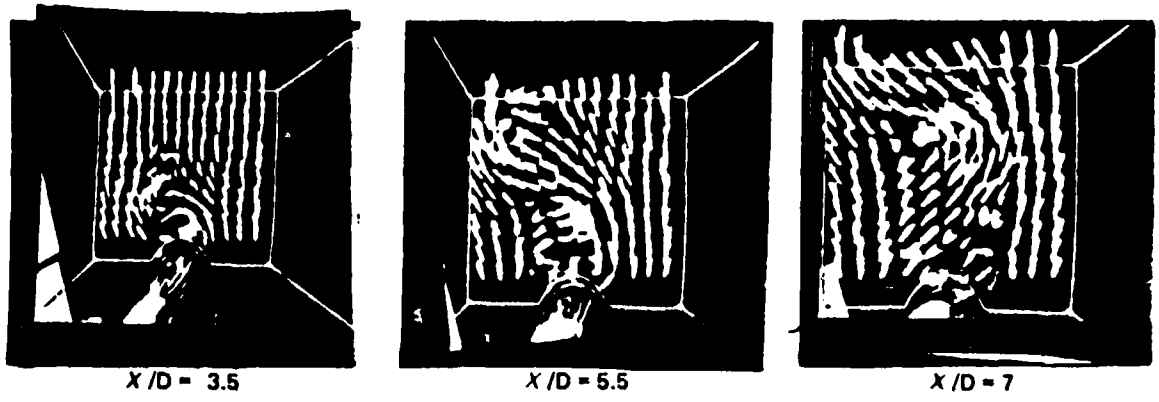

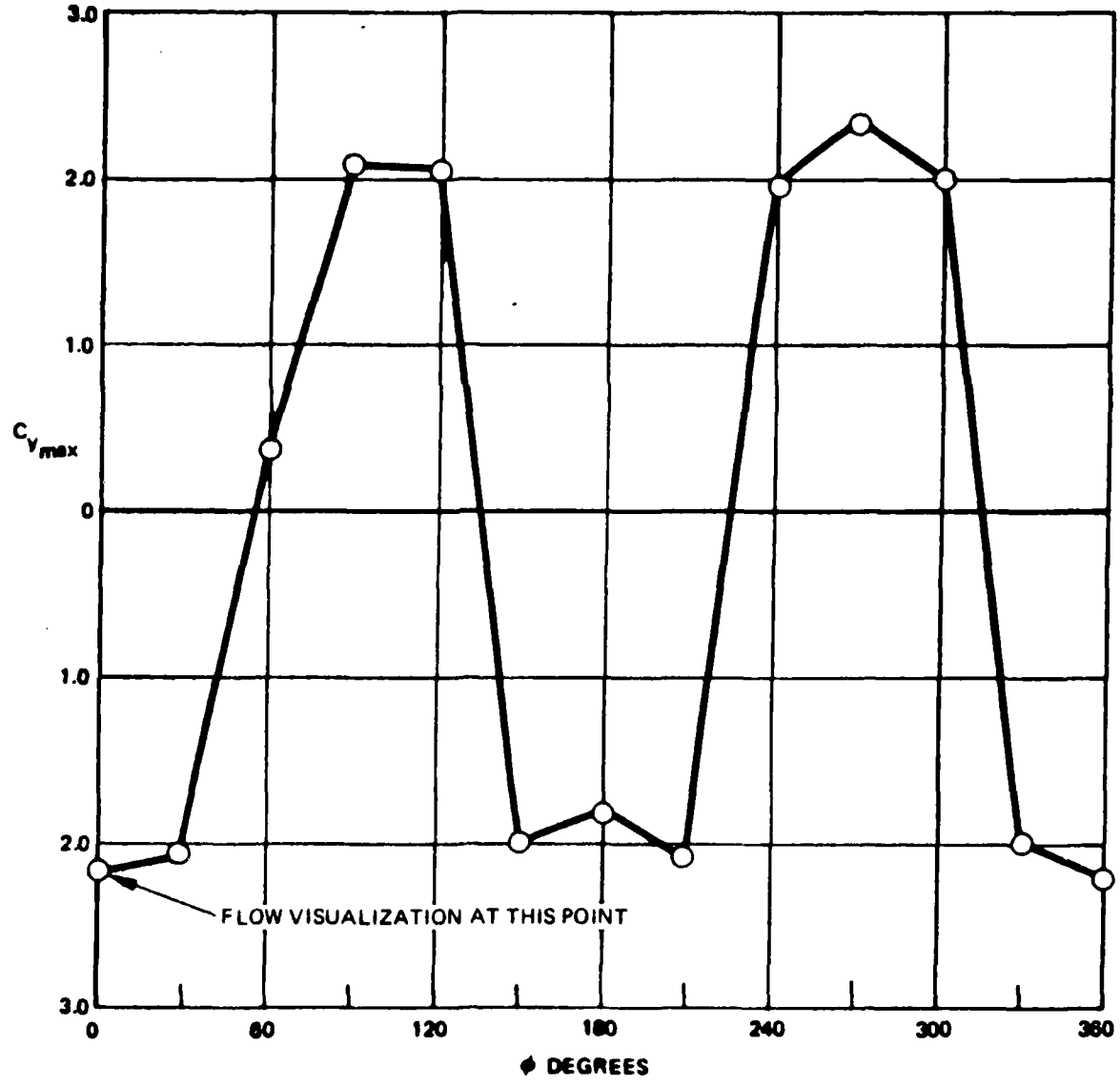

FIG 22 WOOL TUFT PATTERN DEVELOPMENT FOR A 'REGULAR' CASE

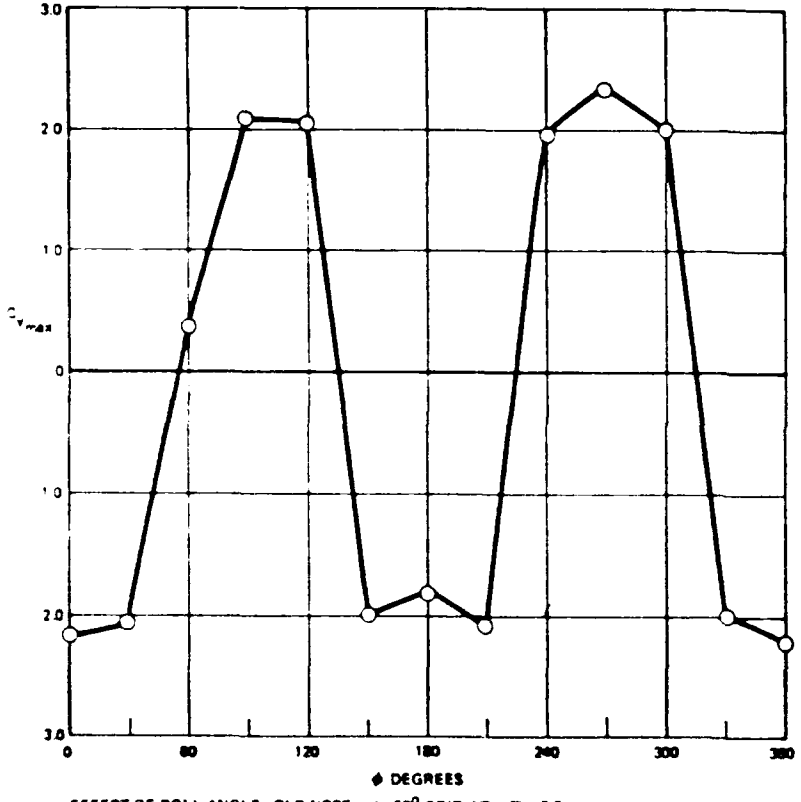

EFFECT OF ROLL ANGLE. OLD NOSE. $\alpha = 50^{\circ}$ GRID AT $X/D = 5.5$

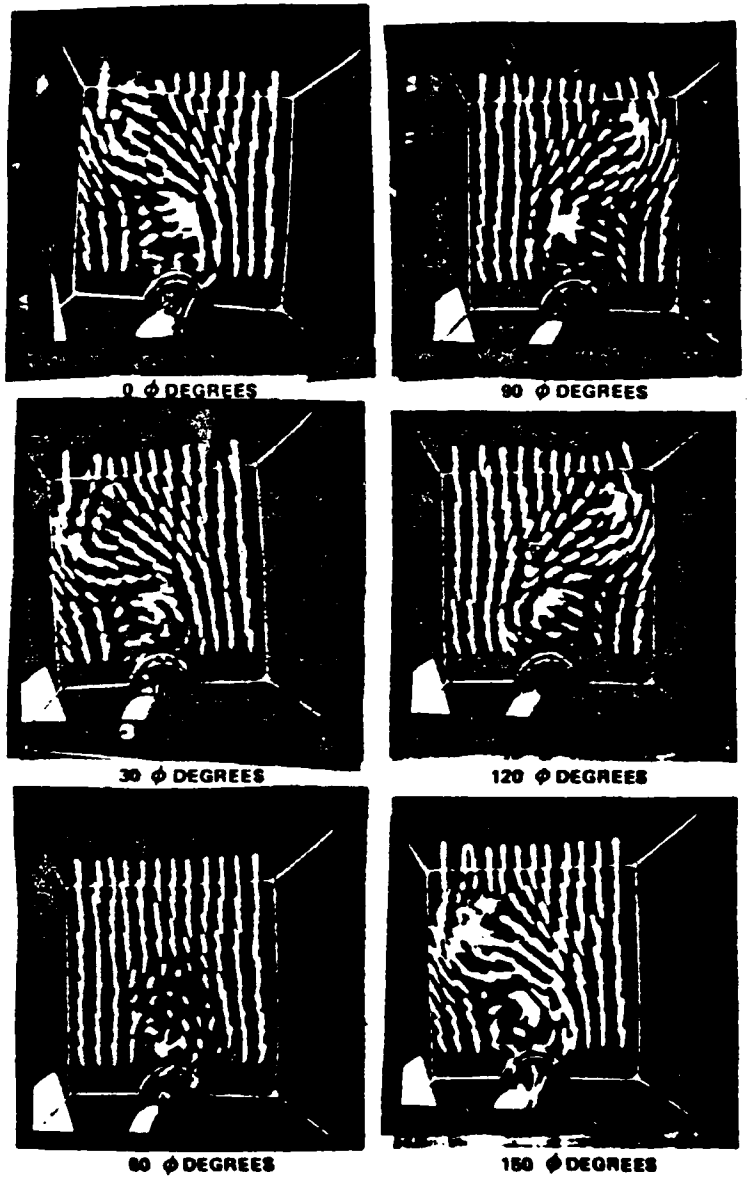

FIG 23

WOOL TUFT PATTERN AT VARIOUS ROLL ANGLES

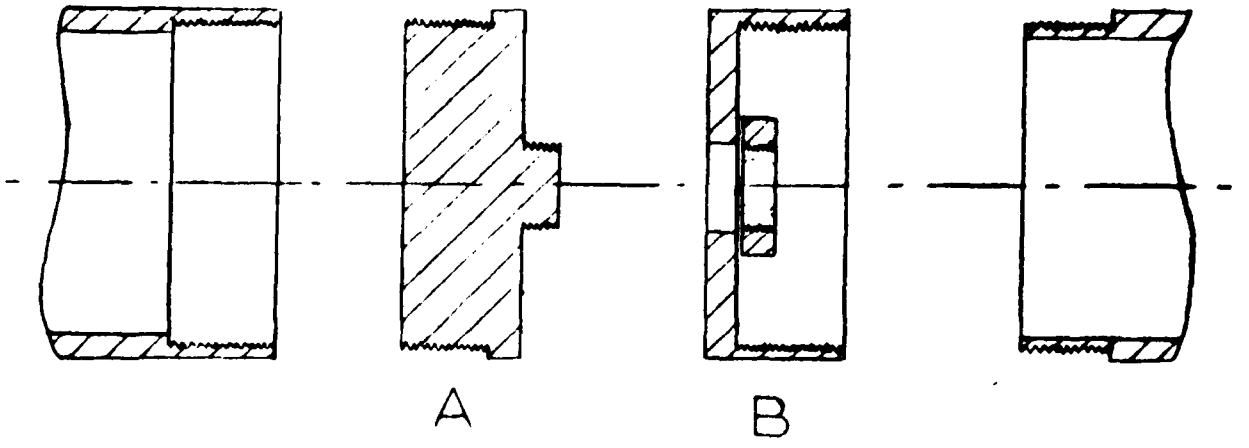
A
B
BODY
NEW SECTION
NOSE

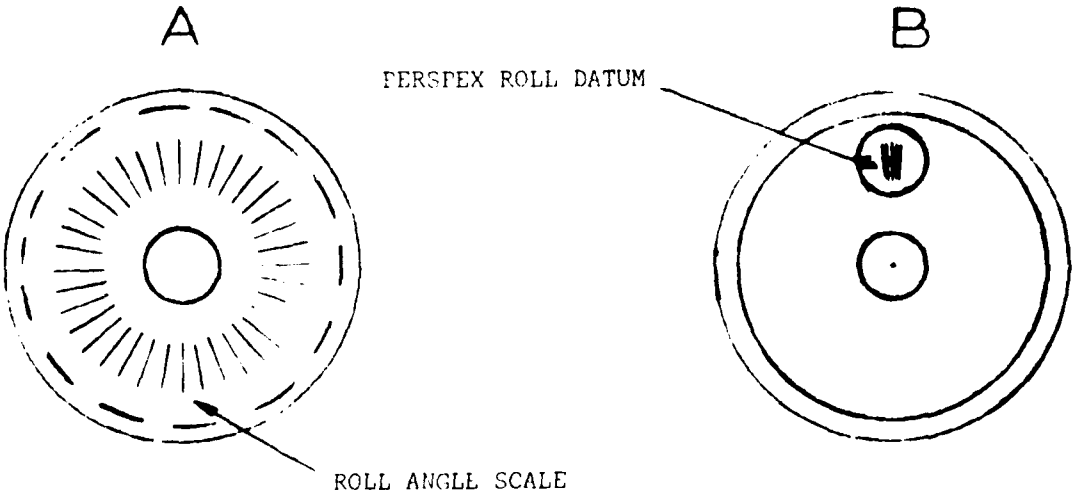
A
B
PERSPEX ROLL DATUM
ROLL ANGLE SCALE

FIG 24